Geochimica et Cosmochimica Acta Vol. 56, pp. 137–154

0016-7037/92/$3.00 + .00

Fluid inclusion gas chemistry in east Tennessee Mississippi Valley-type districts: Evidence for immiscibility and implications for depositional mechanisms*

H. D. JONES and S. E. KESLER
Department of Geological Sciences, University of Michigan, Ann Arbor, MI 48109-1063, USA

(*Received October* 15, 1990; *accepted in revised form October* 30, 1991)

Abstract—Analyses of fluid inclusion gases from Mississippi Valley-type districts in east Tennessee reveal the presence of several distinct aqueous solutions and vapors that were part of the mineralizing process. Inclusion contents were released by crushing 5 to 25 mg mineral samples and by decrepitating individual inclusions; all analyses were obtained by quadrupole mass spectrometry. Most analyzed inclusion fluids consist of H_2O with significant amounts of CH_4 (0.3 to 2.9 mol%), CO_2 (0.1 to 4.7 mol%), and smaller amounts of C_2H_6, C_3H_8, H_2S, SO_2, N_2, and Ar. In general, inclusion gas abundances are greatest for sphalerite from the Mascot-Jefferson City district, lower for the Sweetwater district, and lowest for the Copper Ridge district. Compositional similarities in the inclusion fluids from the three districts imply that mineralization probably formed from fluids that permeated the entire region, rather than from completely separate fluids at each site.

Saturation pressures calculated for these fluid compositions range from 300 to 2200 bars. Burial depths for the host unit have been estimated to be about 2 to 3 km in the east Tennessee area during Devonian time, the age of mineralization indicated by recent isotopic ages. Pressures at these depths, whether hydrostatic or lithostatic, would not have been adequate to prevent phase separation. Thus, our gas analyses represent either a mixture of vapor-rich and liquid-rich inclusions, or liquid-rich inclusions that trapped excess vapor. A lack of visible vapor-rich inclusions, high gas contents in individual fluid inclusion gas analyses obtained by decrepitation, and a positive correlation between decrepitation temperature and gas content for individual inclusions strongly suggest that the samples contain liquid-rich inclusions that trapped varying amounts of excess vapor. This excess gas probably accounts for the anomalously high homogenization temperatures and the wide range of homogenization temperatures observed in fluid inclusions in these ores. The vapor phase could have formed either by phase separation resulting from over-pressured aqueous fluids migrating into a region of hydrostatic pressure, or by incorporation of a pre-existing gas cap at the sites of deposition into the invading aqueous fluid.

Exsolution of a vapor phase from the mineralizing brines should cause precipitation of carbonate and sulfide minerals, but reaction path modelling indicates that the resulting sparry dolomite:sphalerite ratios would be too high to form an ore-grade deposit. On the other hand, if the vapor phase was from a pre-existing sour gas cap that was intercepted by a Zn-rich brine, large amounts of sphalerite would precipitate in a fairly small region. Preliminary mass balance calculations suggest that a gas cap of dimensions similar to the individual districts in east Tennessee could have contained enough H_2S to account for the total amount of sphalerite precipitated.

INTRODUCTION

IN THIS PAPER WE REPORT fluid inclusion gas compositions from three east Tennessee Mississippi Valley-type (MVT) districts and discuss insights they provide into conditions that accompanied mineralization. Specific questions outstanding in east Tennessee, as in many other MVT districts, include: What was the ore-fluid composition? How many fluids were present during ore deposition? Was there a vapor phase present? Were secondary fluid inclusions incorporated into ore minerals subsequent to deposition? What was the regional distribution of the fluid(s)?

In a previous study of fluid inclusion gas compositions in the Mascot-Jefferson City district in east Tennessee, HAYNES et al. (1989) reported relatively large concentrations of non-condensable gases. Those data were obtained from analyses of relatively large samples, which limited their usefulness in addressing the questions outlined above. Quadrupole mass spectrometry, which was employed in the present study, can detect much smaller amounts of gas and has provided valuable insights into the processes associated with deposition of MVT ores. Similar quadrupole analyses in other MVT districts have been used to distinguish different inclusion populations (e.g., HOFSTRA et al., 1989), to identify gas unmixing from brines (e.g., NORMAN and SAWKINS, 1987), and to obtain gas compositions for estimation of burial depths (e.g., BOURCIER, 1986).

EAST TENNESSEE MVT MINERALIZATION

MVT deposits, which are found throughout the Valley and Ridge province of the southern Appalachians, are hosted primarily by Lower Paleozoic carbonate rocks (HOAGLAND, 1976). The Mascot-Jefferson City (zinc), Sweetwater (barite/fluorite), and Copper Ridge (lead/zinc) MVT districts (Fig. 1), which are the focus of this study, are the largest of these deposits. Mineralization in all three districts is in the upper

* Presented at PACROFI III, Third Biennial Pan-American Conference on Research on Fluid Inclusions, held in Toronto, Canada, May 20–22, 1990.

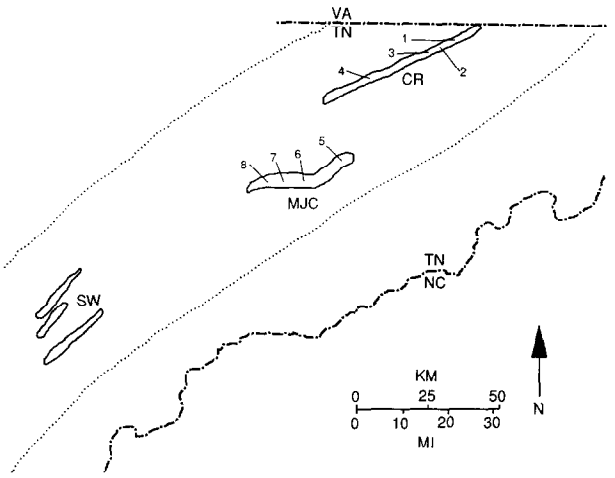

FIG. 1. Location map of the Mascot-Jefferson City (MJC), Sweetwater (SW), and Copper Ridge (CR) districts in east Tennessee. Dotted lines show the approximate boundaries of the Valley and Ridge thrust belt region. Specific mine locations: (1) Eidson; (2) Shiloh; (3) Big War Creek; (4) Idol; (5) Coy; (6) New Market; (7) Young; (8) Immel.

part of the Lower Ordovician Knox Group below a widespread unconformity and is associated with karst and breccia structures (CRAWFORD and HOAGLAND, 1968; MCCORMICK et al., 1971).

ROEDDER (1971), TAYLOR et al. (1983), ZIMMERMAN and KESLER (1981), and CALESS (1983) demonstrated that fluid inclusions in east Tennessee MVT districts homogenize at 100 to 180°C and have salinities of 17.5 to 22 eq. wt% NaCl. KESLER et al. (1988) used $^{87}Sr/^{86}Sr$ ratios in gangue minerals at Mascot-Jefferson City along with an isotopic evolution model to show that the Ordovician Sevier basin and underlying Cambrian and Lower Ordovician sediments were a likely source for the mineralizing fluid. NAKAI et al. (1990) dated Mascot-Jefferson City sphalerite by the $^{87}Rb/^{86}Sr$ method and obtained an age of 380–400 Ma (Devonian), corresponding to the Acadian Orogeny in the Appalachians.

At Mascot-Jefferson City the only economic mineral is sphalerite, but there is abundant associated gangue sparry dolomite, and minor calcite, quartz, and fluorite. Pyrite, galena, and barite are rare. Prior to mineralization at Mascot-Jefferson City there was substantial replacement of recrystalline dolomite by authigenic K-feldspar and silica, which formed an interconnected network around detrital feldspar cores (HEARN and SUTTER, 1985). This was followed by several episodes of sparry dolomite precipitation, which formed before, during, and especially after major sphalerite precipitation (EBERS and KOPP, 1979; CALESS, 1983). Sphalerite forms alternating dark and light bands in some samples, and some additional sphalerite was precipitated in late vugs. Small amounts of fluorite, calcite, and quartz were also deposited late in vugs on some sphalerite crystals (CALESS, 1983). Copper Ridge is similar to Mascot-Jefferson City, but contains more galena. In contrast to these two districts, Sweetwater contains only minor sphalerite and galena that preceded main-stage early fluorite, barite, and late-stage fluorite precipitation (ZIMMERMAN and KESLER, 1981).

EXPERIMENTAL PROCEDURE

Quadrupole Mass Spectrometer Operating Procedure

Analyses of gases in fluid inclusions were made with a VG SXP 600 quadrupole mass spectrometer. Gases were passed for analysis through an inlet system designed to minimize the path distance between sample and ionizing filament (Fig. 2). Source electron energy was 50 volts. Ionized molecules and molecular fragments were detected by a secondary electron multiplier operated at 1200 volts. For most samples, 16 masses were monitored, allowing simultaneous real time analysis for a number of compounds including H_2O, CO_2, CO, CH_4, C_2H_6, C_3H_8, N_2, Ar, H_2S, and SO_2. Data were collected at a rate of approximately 100 cycles per minute.

Gas Liberation Methods

For most analyses inclusion gases were liberated by crushing the host mineral under vacuum with a modified Nupro valve. These analyses, subsequently referred to as *crush* analyses, were usually performed on 5 to 25 mg of an inclusion-hosting mineral. Crush analyses of specific inclusion types in Mascot-Jefferson City sphalerite were performed on selected small portions of fluid inclusion plates that had been determined under microscope to contain predominantly one type of inclusion. Figure 3a shows a typical signal response for a crush analysis. In almost all instances, water mass responses were 2 to 4 orders of magnitude above background; smaller, but significant, signals were obtained for masses corresponding to less abundant gases. Despite the short path length on the inlet system, adsorption of water occurs, as indicated by the longer time required for masses 18, 17, and 16 to drop to background (Fig. 3a). Thus, the signal for each mass must be integrated across the entire scan between the crush and the time at which water peaks return to initial background levels, which typically requires 3 to 4 minutes.

In *individual burst* analyses, inclusion fluids were released by heating small samples under vacuum in a Vycor tube until their inclusions decrepitated. Gases liberated in this manner passed directly into the quadrupole source and produced episodic signal bursts that probably represent individual inclusions (Fig. 3b). To speed the cycling rate of the quadrupole, only masses corresponding to H_2O, CO_2, and CH_4 were monitored in these runs. The faster cycling rate ensured that inclusion bursts lasting only a few seconds spanned at least 10 to 20 cycles, which provides a clear record for analysis.

Gas-rich or vapor inclusions will have low-sloped isochores and should survive without decrepitating to higher temperatures than aqueous inclusions. To test for the presence of vapor inclusions in samples, some crush analyses were performed on splits of samples

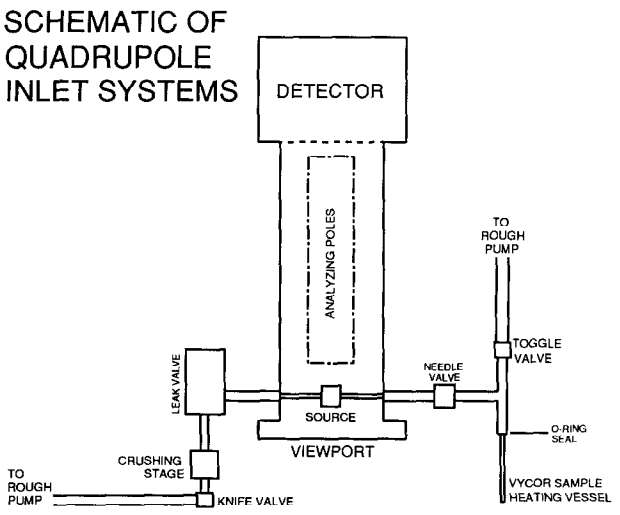

FIG. 2. Schematic diagram of the inlet systems on the University of Michigan quadrupole mass spectrometer.

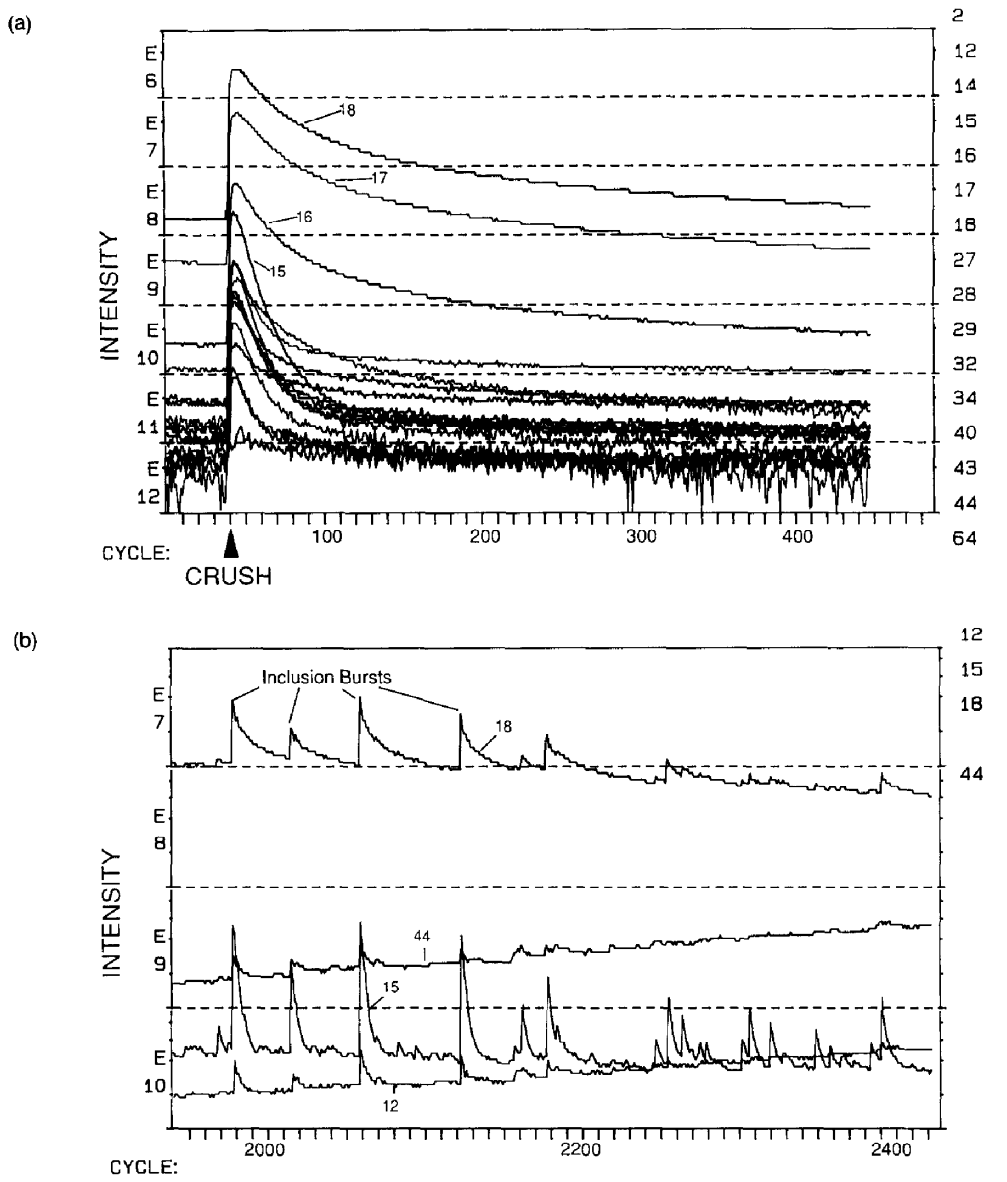

FIG. 3. Signal responses from quadrupole analyses. Vertical scale is the negative logrithm of the SEM current. Horizontal scale is the number of cycles (time into run), ten cycles per tick mark. Masses monitored are listed in the columns at the right, with some individual masses identified on the output. (a) Typical crush analysis response. This sample was crushed on cycle 40. (b) Responses from individual inclusion bursts during a thermal decrepitation run.

that had been heated to 350°C to decrepitate and drive off fluids from liquid-rich inclusions; these analyses are subsequently referred to as *baked* analyses. The material was then cooled and analyzed by crushing, as outlined above, to determine the composition of the surviving inclusions.

Comparison of Quadrupole Results and Previous Analyses

Inclusion compositions determined in this study differ significantly from gas analyses reported by HAYNES et al. (1989). We report less CO_2, less N_2, and much more CH_4 from the same or similar samples. HAYNES et al. (1989) liberated gases for analysis by heating 1 g of sphalerite to 350°C to decrepitate inclusions, and then transferred the entire amount of released gas to a gas chromatograph. Their higher CO_2 values may have resulted from decomposition of small amounts of organic matter and/or carbonate material during the heating procedure. Our investigations demonstrate that CO_2 is released continually as a sample is heated, in addition to the episodic spiked release pattern typical of fluid inclusion bursts (note the traces of masses 44 and 12 in Fig. 3b). This noninclusion-derived CO_2 does not contribute to our individual burst compositions because released gases pass continuously into the quadrupole source without accumulating, and we subtract the background that exists for each mass immediately before each burst from the integrated signal used to determine the composition of the burst. Neither of these options was available to HAYNES et al. (1989). All of the noninclusion-related CO_2 generated during heating in their runs was analyzed and incorporated into the reported composition. In quadrupole runs in which we duplicated the approach of heating sphalerite to 350°C and then analyzing the bulk gas released, all but one analysis yielded more than 1 mol% CO_2. In contrast, very few of our crush or individual burst analyses yielded more than 0.5 mol% CO_2.

Few of our analyses yielded N_2, whereas HAYNES et al. (1989) detected N_2 in all of their sphalerite analyses, in amounts ranging from 0.05 to 0.62 mol%. The discrepancy may have resulted from their treatment of samples with acetonitrile prior to analysis in an

attempt to remove organic contamination (ALEXANDROVSKA et al., 1980). In our analyses using the same method, N_2 was detected in amounts ranging from 0.01 to 0.94 mol% on splits of their original sample material. N_2 was not detected during similar analysis of sphalerite that was not pretreated with acetonitrile. No samples employed in this study were pretreated before analysis.

The vast difference in amounts of CH_4 detected by the two techniques is not so easily explained. We have not observed that CH_4 is produced or destroyed by heating the samples before analysis. Although some of our quadrupole samples analyzed in bulk after heating yielded no CH_4, others yielded 0.49 and 0.54 mol%, values that are in the range we detected in our normal crush analyses. In all of our analyses of east Tennessee sphalerite we rarely report less than 0.2 mol% CH_4, whereas HAYNES et al. (1989) never detected more than 0.06 mol% CH_4. Our quadrupole crush analysis method does not result in large detected amounts of CH_4 for all types of samples. For instance, crush analyses of the Hansonburg fluorite "standard" HF-1 rarely yielded more than 100 ppm CH_4, an amount similar to the value originally reported (91 ppm) by NORMAN et al. (1985). Thus, while there is no obvious explanation for the difference in amounts of CH_4 reported here and by HAYNES et al. (1989), we believe the previous study consistently underreported CH_4 by more than an order of magnitude.

Analytical Considerations

Determination of mole percentages from raw data

Comparing intensities of only parent peaks for individual gases will not yield an accurate overall gas composition for two major reasons. First, most gases are "cracked" to some extent into smaller fragments at the quadrupole analyzer source. Secondly, some gases (e.g., N_2 and CO) share the same parent mass; if only mass 28 were analyzed, N_2 and CO could never be distinguished. Fortunately, the resulting cracked fragments are also ionized and detected, allowing one to determine the total amount of gas originally present. By knowing the cracking "pattern" (relative intensities of parent and cracked peaks at a particular pressure) of each gas, it is possible to distinguish among gases. In the case of N_2 and CO, monitoring the following masses allows us to obtain analyses of each: *28* (parent mass—N_2^+ and CO^+); *16* (O^+ from CO); *14* (N^+ and N_2^{++} from N_2); and *12* (C^+ from CO).

While tables of cracking patterns for gases are available in the literature, the patterns are dependent on operating conditions and inlet/source geometry and should be determined for each individual instrument. We have determined cracking patterns on pure gases for all of the compounds reported in analyses in this paper under constant operating conditions, and for a variation of several orders of magnitude pressure in the analyzer. Some gases show widely varying (but consistent) cracking patterns with variations in pressure; for a given species this effect does not seem to depend on what mixture of gases is present in the analyzer, but probably just reflects the effect of competition for available electrons in the quadrupole source. We expect to publish a full account on the effects of analyzer pressure on cracking patterns and determined relative sensitivities (discussed below) in a later paper. For all of our analyses we have used cracking patterns appropriate for the pressures generated by the fluid inclusion gases upon crushing or decrepitation.

Determination of the relative abundances (mole fraction) of gases in a complex gas mixture requires use of a matrix fitting procedure, provided as part of the operating software with the quadrupole. The program takes into account cracking patterns for each gas in the analysis and delineates multiple contributions to masses by a series of simultaneous equations in a matrix—one side of the matrix has a list of all gases considered in the analysis, the other side has a list of all masses that were monitored. In the appropriate cells are the known relative intensities of masses from each gas cracking pattern; these are compared to the overall signal detected for each mass and partitioned to the appropriate gases to determine the original composition in mol%. A correlation coefficient determined for each analysis defines how well the reported final composition fits the original raw data; a low correlation coefficient indicates either a bad analysis or that another gas component not accounted for in the data reduction was present. This last possibility is discounted by initially performing full scans of all masses present in similar samples to determine whether we are analyzing for the correct mixture of gases.

Determination of relative sensitivities of individual gases

Because of several analytical effects, including varying probabilities of ionization and detection sensitivities, equal amounts of different gases will not result in the same reported signal by the quadrupole. One can determine the "relative" sensitivities of the instrument to various gases for given pressures in the analyzer. Usually these sensitivities are reported relative to N_2, which is assigned a relative sensitivity of 1.000. Tables of both theoretical and empirical relative sensitivities are available in the literature, but, like cracking patterns, these values should be determined for each instrument under specific operating conditions. We have determined relative sensitivities of each gas reported in this study by making multiple runs of 50:50 molar mixtures of all gases (except H_2O) with N_2 and determining the instrumental response across a wide variety of pressures. As with cracking patterns there can be a substantial variation in relative sensitivity of a particular gas with pressure; for this study we have employed the appropriate values for pressures attained during our analyses.

The nature of H_2O makes it impossible to manufacture 50:50 mixtures with N_2 as we did with other gases. Literature values of H_2O relative sensitivity are very close to 1.000; this value is what we have used in our data reduction. A relative sensitivity value for H_2O can also be determined indirectly by comparison with another gas for which the relative sensitivity has been determined by the first technique. Using coldfingers on a second inlet system, we introduced a known amount of CO_2 and H_2O into the quadrupole, and using our relative sensitivity values that we have employed for data reduction, we obtained a reasonably close match with the expected value: for an initial mixture of 82.1% H_2O and 17.9% CO_2 we obtained a value of 81% H_2O in the analysis.

Although "standards" that mimic releasing fluids from inclusions are not available, we have run commercially prepared pre-analyzed gas mixtures and obtained good results using our determined values for cracking patterns and relative sensitivities. For minor species (less than 1 mol%), our values usually differed only a few percent from the *reported* amount listed for the mixtures, and rarely more than 5% of the reported amount. We have also run crush analyses on a Hansonburg fluorite "standard" supplied to us by David Norman and obtained compositions similar to those he reports (NORMAN et al., 1985). We have attempted to analyze synthetic H_2O-CO_2 inclusions in quartz, but have not obtained good results from these samples because they contain 2 to 3 orders of magnitude less total fluid than the natural samples we run, and the signal-to-background ratio was very low.

The problem of H_2O adsorption during analysis

Reliable determinations of the amount of H_2O present in a sample have long been a problem in many analytic techniques, and the quadrupole approach we have employed in this study is no exception. Confidence in the amount of H_2O reported in analyses is of particular concern to us, because of the high amounts of other gases (primarily CH_4 and CO_2) that we have obtained, and the trends of these gases with H_2O. These results could be artifacts of the analytic technique if we were either consistently overreporting the amounts of non-H_2O gases, or underreporting the amount of H_2O. Extensive investigation into the effects of variations of cracking patterns and relative sensitivities of gases on reported gas compositions makes it clear that we are not overestimating non-H_2O gases in our analyses. However, because of the occurrence of adsorption, underestimation of H_2O is possible, and if it is a serious problem that occurs randomly to varying degrees, it might account for the observed H_2O-gas trends that we report in this study. There are several reasons we do not believe analytic error due to H_2O adsorption is responsible for the observed trends.

(1) On many of our samples, particularly sphalerite from the Mascot-Jefferson City district, we performed duplicate crush analyses on small portions of crystal that were immediately adjacent to one

TABLE 1. FLUID INCLUSION COMPOSITIONS FROM UNBAKED MASCOT-JEFFERSON CITY CRUSH ANALYSES (MOLE PERCENT)

1A. UNZONED, DARK, AND LIGHT SPHALERITE

SAMPLE	H2O	CO2	CO	CH4	C2H6	C3H8	N2	Ar	H2S	SO2
UNZONED										
C39SP1X	96.4	0.73	0.18	2.45	0.000	0.111	0.000	0.0058	0.0200	0.0140
C39SP2X	97.2	0.23	0.06	2.18	0.208	0.077	0.000	0.0069	0.0180	0.0083
C39SP3X	97.1	0.15	0.03	2.37	0.210	0.105	0.000	0.0083	0.0170	0.0070
C6SP1X	98.0	0.24	0.06	1.38	0.000	0.238	0.000	0.0001	0.0160	0.0085
C6SP2X	97.7	0.31	0.09	1.64	0.106	0.092	0.000	0.0046	0.0140	0.0053
C6SP3X	97.6	0.29	0.07	1.79	0.109	0.096	0.000	0.0055	0.0130	0.0062
I32SP1X	98.1	0.50	0.10	1.13	0.000	0.078	0.000	0.0039	0.0140	0.0084
I32SP2X	97.2	0.26	0.09	2.15	0.000	0.180	0.000	0.0006	0.0200	0.0091
I32SP3X	98.1	0.21	0.11	1.36	0.024	0.145	0.000	0.0046	0.0120	0.0048
Y21SP1X	98.2	0.36	0.08	1.24	0.048	0.057	0.000	0.0037	0.0160	0.0086
Y21SP2X	97.6	0.48	0.10	1.55	0.083	0.116	0.000	0.0056	0.0140	0.0070
Y21SP3X	98.5	0.19	0.06	1.08	0.000	0.149	0.000	0.0000	0.0130	0.0066
DARK										
I18DSP1X	97.1	0.24	0.04	2.19	0.160	0.151	0.000	0.0071	0.0170	0.0140
I18DSP2X	96.7	0.17	0.05	2.49	0.221	0.292	0.000	0.0110	0.0170	0.0100
I18DSP3X	98.0	0.14	0.16	1.39	0.025	0.228	0.000	0.0072	0.0190	0.0095
N44DSP1X	98.5	0.25	0.09	1.04	0.030	0.049	0.000	0.0042	0.0150	0.0086
N44DSP2X	97.2	0.16	0.10	2.23	0.000	0.168	0.023	0.0011	0.0160	0.0084
N44DSP3X	97.2	0.29	0.22	1.93	0.005	0.251	0.000	0.0085	0.0170	0.0089
N96DSP1X	97.3	0.66	0.10	1.68	0.121	0.143	0.000	0.0086	0.0037	0.0024
N96DSP2X	97.6	0.29	0.09	1.64	0.000	0.389	0.000	0.0006	0.0110	0.0066
N96DSP3X	97.8	0.40	0.12	1.39	0.000	0.210	0.000	0.0005	0.0120	0.0054
Y49DSP1X	97.9	0.40	0.15	1.34	0.058	0.056	0.000	0.0058	0.0260	0.0130
Y49DSP2X	98.7	0.22	0.09	0.85	0.027	0.034	0.000	0.0028	0.0220	0.0083
LIGHT										
I18LSP2X	98.9	0.15	0.07	0.67	0.033	0.065	0.000	0.0040	0.0150	0.0110
I18LSP3X	98.7	0.15	0.08	0.87	0.066	0.092	0.000	0.0054	0.0140	0.0089
N44LSP1X	98.2	0.25	0.14	1.27	0.000	0.093	0.000	0.0025	0.0250	0.0130
N44LSP2X	98.0	0.23	0.15	1.40	0.000	0.079	0.000	0.0029	0.0250	0.0120
N44LSP3X	99.5	0.05	0.04	0.32	0.000	0.020	0.007	0.0006	0.0071	0.0026
N96LSP1X	97.6	0.44	0.17	1.54	0.000	0.148	0.000	0.0038	0.0250	0.0120
N96LSP2X	97.7	0.98	0.07	1.11	0.041	0.058	0.000	0.0035	0.0160	0.0085
N96LSP3X	97.9	0.44	0.11	1.34	0.071	0.096	0.000	0.0055	0.0160	0.0090
Y49LSP1X	99.5	0.06	0.04	0.37	0.000	0.030	0.008	0.0008	0.0085	0.0037
Y49LSP2X	99.4	0.06	0.05	0.40	0.000	0.029	0.000	0.0007	0.0073	0.0029
Y49LSP3X	97.9	0.28	0.20	1.38	0.000	0.101	0.000	0.0025	0.0230	0.0100
AVERAGE										
UNZONED	97.6	0.33	0.09	1.69	0.066	0.120	0.000	0.0041	0.0156	0.0078
DARK	97.6	0.29	0.11	1.65	0.059	0.179	0.002	0.0052	0.0160	0.0086
LIGHT	98.5	0.28	0.10	0.97	0.019	0.074	0.001	0.0029	0.0165	0.0085

FIRST LETTER OF SAMPLE NAME: C = COY MINE I = IMMEL MINE
N = NEW MARKET MINE Y = YOUNG MINE

1B. SPHALERITE CONTAINING PREDOMINANTLY ONE SPECIFIC INCLUSION TYPE

SAMPLE	H2O	CO2	CO	CH4	C2H6	C3H8	N2	Ar	H2S	SO2
TYPE I										
Y-58A1X	97.5	0.22	0.16	1.78	0.117	0.124	0.006	0.0093	0.0250	0.0240
Y-58A2X	96.7	0.26	0.14	2.31	0.155	0.080	0.194	0.0120	0.0200	0.0170
Y-61A1X	96.7	0.23	0.05	2.54	0.183	0.146	0.000	0.0100	0.0290	0.0300
Y61A2X	98.5	0.20	0.10	0.98	0.044	0.031	0.003	0.0089	0.0210	0.0200
Y9A2X	99.0	0.15	0.05	0.60	0.034	0.027	0.075	0.0073	0.0150	0.0150
TYPE II										
Y2VA1X	99.5	0.09	0.06	0.27	0.000	0.025	0.000	0.0039	0.0130	0.0130
Y-58V1X	98.9	0.16	0.07	0.72	0.025	0.071	0.025	0.0081	0.0150	0.0140
Y-58V2X	98.7	0.14	0.07	0.92	0.034	0.028	0.019	0.0056	0.0170	0.0130
Y-61V1X	99.1	0.18	0.07	0.54	0.020	0.038	0.000	0.0062	0.0160	0.0140
Y-61V2X	98.3	0.18	0.07	1.23	0.053	0.038	0.060	0.0046	0.0230	0.0190
Y9V2X	97.3	0.48	0.00	1.23	0.104	0.183	0.567	0.0170	0.0280	0.0240
TYPE III										
Y2S1X	99.6	0.19	0.00	0.00	0.025	0.011	0.142	0.0076	0.0210	0.0190
Y61AV1X	97.6	0.52	0.15	1.31	0.108	0.136	0.014	0.0120	0.0160	0.0240
Y61SA1X	96.0	0.33	0.18	2.90	0.189	0.097	0.158	0.0140	0.0390	0.0160
Y61SV1X	99.3	0.10	0.04	0.43	0.018	0.021	0.052	0.0038	0.0120	0.0120
Y61SV2X	98.0	0.36	0.12	1.34	0.055	0.054	0.000	0.0081	0.0280	0.0270
Y61SV3X	96.2	0.50	0.16	2.71	0.181	0.092	0.048	0.0160	0.0180	0.0220
Y61VS1X	99.1	0.11	0.02	0.54	0.022	0.029	0.100	0.0062	0.0110	0.0180
Y61VS2X	97.2	0.41	0.12	1.95	0.108	0.045	0.035	0.0088	0.0220	0.0110
AVERAGE										
TYPE I	97.7	0.21	0.10	1.64	0.107	0.082	0.056	0.0095	0.0220	0.0212
TYPE II	98.6	0.21	0.05	0.82	0.039	0.064	0.112	0.0076	0.0187	0.0162
TYPE III	97.9	0.31	0.10	1.40	0.088	0.061	0.069	0.0096	0.0209	0.0186

1C. SPARRY DOLOMITE

SAMPLE	H2O	CO2	CO	CH4	C2H6	C3H8	N2	Ar	H2S	SO2
C39D3X	96.5	2.05	0.14	1.16	0.015	0.030	0.000	0.0040	0.0200	0.0080
C6D1X	96.0	2.32	0.12	1.36	0.018	0.044	0.000	0.0039	0.0270	0.0130
C6D2X	96.4	2.05	0.13	1.29	0.012	0.041	0.000	0.0048	0.0210	0.0110
C6D3X	96.3	2.15	0.10	1.26	0.012	0.041	0.000	0.0040	0.0230	0.0100
I18D1X	96.4	2.21	0.09	1.16	0.026	0.046	0.000	0.0043	0.0260	0.0130
I18D2X	97.0	1.69	0.07	1.05	0.027	0.039	0.000	0.0029	0.0210	0.0130
I18D3X	96.6	2.11	0.07	1.04	0.027	0.038	0.000	0.0024	0.0230	0.0110
I32D1X	92.7	4.73	0.06	2.30	0.033	0.035	0.000	0.0047	0.0240	0.0120
I32D2X	95.0	3.85	0.02	1.02	0.022	0.022	0.000	0.0025	0.0160	0.0077
I32D3X	96.3	2.71	0.02	0.92	0.027	0.019	0.000	0.0020	0.0150	0.0068
N44D1X	99.2	0.37	0.04	0.29	0.000	0.017	0.000	0.0008	0.0071	0.0034
N44D2X	97.0	1.49	0.08	1.24	0.018	0.040	0.000	0.0031	0.0230	0.0110
N44D3X	99.3	0.30	0.04	0.29	0.000	0.015	0.000	0.0007	0.0063	0.0027
N96D1X	99.2	0.49	0.02	0.20	0.004	0.009	0.000	0.0010	0.0065	0.0034
N96D2X	97.6	1.35	0.08	0.81	0.010	0.040	0.000	0.0029	0.0200	0.0098
N96D3X	97.8	1.27	0.08	0.73	0.008	0.026	0.000	0.0020	0.0210	0.0081
Y21D1X	94.9	2.75	0.03	2.20	0.015	0.041	0.000	0.0039	0.0230	0.0150
Y21D2X	94.5	3.22	0.03	2.10	0.013	0.037	0.000	0.0035	0.0200	0.0120
Y21D3X	97.4	1.71	0.10	0.72	0.004	0.025	0.000	0.0033	0.0160	0.0083
AVERAGE	96.6	2.04	0.07	1.11	0.015	0.032	0.000	0.0030	0.0189	0.0094

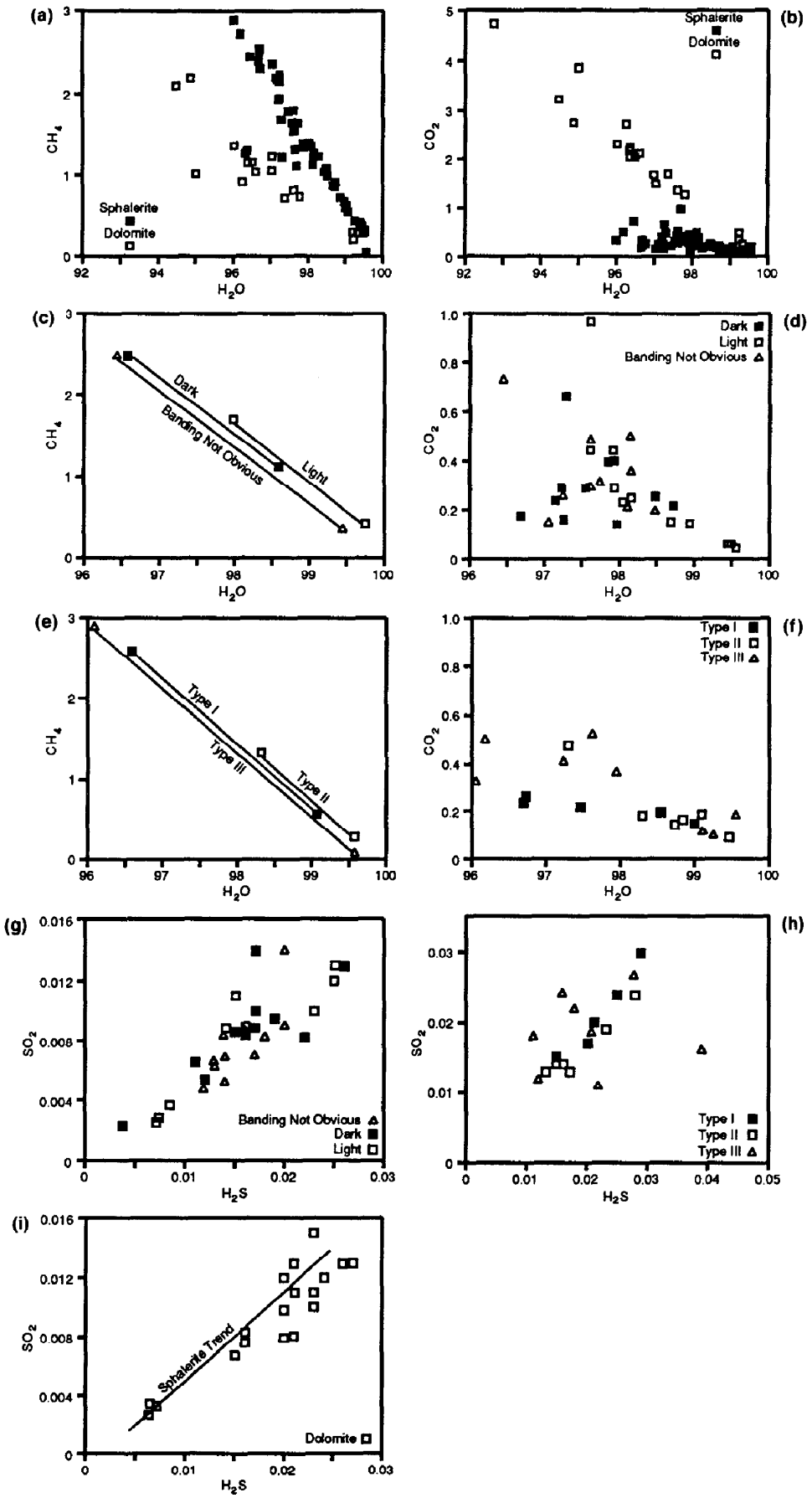
(a)
CH4
H2O
Sphalerite
Dolomite
(b)
CO2
H2O
Sphalerite
Dolomite
(c)
CH4
H2O
Dark
Banding Not Obvious
Light
(d)
CO2
H2O
Dark
Light
Banding Not Obvious
(e)
CH4
H2O
Type I
Type III
Type II
(f)
CO2
H2O
Type I
Type II
Type III
(g)
SO2
H2S
Banding Not Obvious
Dark
Light
(h)
SO2
H2S
Type I
Type II
Type III
(i)
SO2
H2S
Sphalerite Trend
Dolomite

another. These duplicate analyses, which are reported in the tables as 1X, 2X, etc. (last two characters of the sample name), contain comparable amounts of non-H_2O gases (either gas-rich, gas-moderate, or gas-poor), and do not span the entire range of CH_4 contents obtained from the general data set. Application of the statistical data test described by GARRETT (1969) to our duplicate analyses yields a 90% confidence that the compositional ranges are due to actual sample differences, and not just to analytic variability.

(2) As outlined above, masses of interest are monitored in crush analyses until the responses for the H_2O masses have decayed to or near the values present before the crush. We then integrate the H_2O response across the entire run up to that point. To some extent, the determination of where to end the analysis is arbitrary, and variations in the endpoint will have an effect on the amount of H_2O reported for the analysis. This effect is small at the point at which we actually cut the analyses, however. As an example, manipulation of data files has shown that to erroneously report an amount of H_2O corresponding to one of our gas-rich analyses (around 96.5 mol%) from one of our gas-poor analyses (>99 mol%), we would have to cut the H_2O integration at a point corresponding to approximately cycle 100–150 on Fig. 3a, which is well before the H_2O response has begun to approach the original background values.

(3) In thermal decrepitation analyses, individual burst compositions above 400°C show increasing non-H_2O gas contents with higher temperature, a correlation we relate to differing internal pressures in the inclusions of different gas compositions. If adsorption is responsible for the range in reported compositions, the effect should be the reverse of what we have observed: adsorption would be expected to be greater at lower temperatures on the sample and decrepitation inlet system, resulting in gas-rich (H_2O-low) compositions at low temperatures changing to gas-poor compositions at high temperatures.

Thus, while H_2O-adsorption on the crystal and in the inlet system can be a problem, we do not think it is responsible for either the high gas contents we report in many analyses, or the linear binary trends of some of these gases with H_2O abundance.

FLUID COMPOSITIONS

Mascot-Jefferson City District

Types of fluid inclusions

Mascot-Jefferson City sphalerite contains three types of visually distinguishable inclusions, which we attempted to characterize with quadrupole mass spectrometer analyses. *Type I* inclusions are primary two-phase (liquid plus a vapor bubble), spatially isolated inclusions, analogous to those employed by TAYLOR et al. (1983) in their heating/freezing inclusion study of the district. Most Type I inclusions are only a few micrometers in diameter, although some are as large as 30 μm. *Type II* inclusions are small (1 to 2 μm) and spherical, and almost opaque due to high internal reflection. They are often, but not always, aligned along planes, and are obviously later than Type I inclusions. It is not clear that Type II inclusion planes cross sphalerite grain boundaries, and they could be coeval with sphalerite. Crushing stage tests on Type II inclusions have not indicated that they are vapor inclusions. *Type III* inclusions are found in deformed sphalerite and commonly appear as smeared brown patches tens of micrometers in length. They are often not immediately recognizable as inclusions, but vapor bubbles occasionally can be seen. Type III inclusions are sometimes aligned with deformational twinning visible under crossed polars.

Crush analyses

Sphalerite. In almost all analyses of Mascot-Jefferson City sphalerite (Tables 1a, b), $H_2O + CH_4 + CO_2$ make up more than 99 mol% of the gas composition, although relative abundances of CH_4 and CO_2 vary greatly among samples. On an H_2O-CH_4 binary (Fig. 4a), all sphalerite fluid compositions plot as a line, with CH_4 ranging from 0.3 to almost 3.0 mol%. On an H_2O-CO_2 binary (Fig. 4b) there is more scatter, but a correlation is apparent. CO_2 rarely exceeds 0.5 mol% in any Mascot-Jefferson City sphalerite analysis. In samples with less than about 0.2 mol% CO_2, the CO_2 and H_2O abundances trend linearly for H_2O values greater than 98.5 mol%. Samples with more than 0.2 mol% CO_2 do not correlate as well with H_2O abundance.

Sphalerite crush analyses from dark, light, or unzoned sphalerite (Fig. 4c) show that dark sphalerite inclusions have greater amounts of CH_4 (0.8–2.5 mol%) than inclusions in light sphalerite (0.3–1.5 mol%). Gas compositions from unzoned sphalerite span almost the entire range (0.4–2.4 mol%). The association of methane with dark sphalerite agrees with the observations of HAYNES et al. (1989). Figure 4d shows that (with one exception) H_2O and CO_2 from light sphalerite vary linearly in the 0.05–0.5 mol% CO_2 range. Dark and unzoned sphalerite do not show linear correlations for H_2O and CO_2, although at H_2O contents greater than 98.5 mol% these samples plot on the light sphalerite line.

Type I- and Type II inclusion–dominated samples yield compositions that occupy different parts of the overall sphalerite trends on the H_2O-CH_4 and H_2O-CO_2 binary plots (Fig. 4e, f). Type I inclusions contain 0.6–2.6 mol% CH_4, while type II inclusions contain only 0.3–1.3 mol% CH_4. In contrast, type III inclusions span the entire range, but do not deviate from the linear trend. Type I and Type II inclusion compositions plot toward the CO_2-rich and CO_2-poor ends, respectively, of a fairly linear trend on the H_2O-CO_2 binary (Fig. 4f). However, Type III inclusion compositions fall either on this line or at higher CO_2 values.

H_2S is present in amounts of 100 to 250 ppm (molar) in Mascot-Jefferson City sphalerite, while SO_2 is less abundant, ranging from 50 to 250 ppm. The average H_2S/SO_2 ratio for crush analyses is 2.07; note the linear trend on the binary (Fig. 4g). There is no apparent difference between dark and light sphalerite. A best-fit correlation line for crush analyses intercepts almost at the origin (1 ppm SO_2) for 0 ppm H_2S. The H_2S-SO_2 binary plot for specific inclusion types (Fig. 4h) looks less linear, but the scatter is due to Type III inclu-

FIG. 4. H_2O-gas binary representations of MJC sphalerite and dolomite analyses (all data on these and subsequent figures in mol%). Note that scales are not constant on the different diagrams. (a) H_2O-CH_4, sphalerite and dolomite crushes. (b) H_2O-CO_2, sphalerite and dolomite crushes. (c) H_2O-CH_4, sphalerite compositional ranges by color. (d) H_2O-CO_2, sphalerite color crushes (e) H_2O-CH_4, sphalerite compositional ranges by inclusion type. (f) H_2O-CO_2, sphalerite crushes of specific inclusion types. (g) H_2S-SO_2, sphalerite crushes. (h) H_2S-SO_2, sphalerite crushes of specific inclusion types. (i) H_2S-SO_2, dolomite crushes.

sions; Type I- and Type II inclusion–dominated samples plot linearly. Other gas compounds are present in only minor amounts in the sphalerite fluids. Higher alkanes (C_2H_6 + C_3H_8) range up to a few hundred ppm, but do not correlate consistently with other compounds. Argon, which was detected in amounts up to 110 ppm, has a weak negative correlation with H_2O, but not with other compounds.

Sparry dolomite. Inclusion gas compositions from Mascot-Jefferson City sparry dolomite crushes (Table 1c and Fig. 4) plot on linear H_2O-CH_4 and H_2O-CO_2 trends (Fig. 4a, b) that differ from those of sphalerite. The dolomite analyses yield much more CO_2 (0.3 to almost 5 mol%), and less CH_4 (0.2–2.3 mol%) than the sphalerite analyses. Average total sulfur gas content is slightly higher in dolomite inclusions (283 ppm), but the H_2S/SO_2 ratio (2.05) is almost identical to that of sphalerite. The H_2S-SO_2 trend in dolomite is essentially indistinguishable from sphalerite in both slope and intercept (Fig. 4i).

Baked sphalerite. Fluid inclusion compositions from baked Mascot-Jefferson City sphalerite crushes (Table 2a) exhibit more variability than unbaked compositions, but still show fairly linear trends on H_2O-CH_4 and H_2O-CO_2 plots (Fig. 5a, b). Note that in both plots the baked sphalerite compositions are displaced from the trend of unbaked sphalerite analyses toward the unbaked sparry dolomite trend; the effect is more pronounced for CO_2 than CH_4. Baked sphalerite shows little to moderate enrichment in CH_4, and moderate to substantial enrichment in CO_2 over unbaked sphalerite. In analyses of baked splits of the three inclusion types (Fig. 5c, d), surviving Type III inclusions have a more CO_2-rich composition than surviving Type I and Type II inclusions; four of the five baked Type III compositions plot on the unbaked dolomite line.

Baked splits from inclusion-specific sphalerite samples show a division in H_2S/SO_2 ratios. Surviving Type I and Type II inclusions yield ratios averaging 0.72 and 0.91, respectively, whereas Type III inclusions average 1.68. Total sulfur (H_2S + SO_2) in baked Type III inclusions is slightly greater than in baked Type I and Type II inclusions (averaging 368 ppm vs. 365 and 335 ppm), but not enough to account for the difference in H_2S/SO_2 values among inclusion types by addition or subtraction of one component. Baked Type I and Type II inclusion–dominated samples trend linearly in H_2S-SO_2 space, but Type III inclusions show no such correlation (Fig. 5f).

Baked sparry dolomite. Baked sparry dolomite samples (Table 2b) do not yield compositions different than unbaked samples. Baked dolomite inclusion compositions plot across almost the entire trend established by unbaked dolomite on both the H_2O-CH_4 and H_2O-CO_2 binary diagrams (Fig. 6a, b). Thus, unlike sphalerite, where baked samples contain different fluids than unbaked samples, there is no evidence for secondary fluids in dolomite.

Individual burst analyses

Compositions of individual inclusions in sphalerite (Table 2c) that burst by thermal decrepitation plot on one of the two lines established by crush analyses of unbaked sphalerite and dolomite on both the H_2O-CH_4 and H_2O-CO_2 binaries (Fig. 7a, b); individual bursts plot on either the sphalerite or dolomite line with respect to both CH_4 and CO_2. For most sphalerite samples, all integrated individual bursts plot on either the sphalerite or dolomite line, but one sample (118LSP5) had separate bursts that plot on both lines, indicating that some sphalerite inclusions contain what must be considered to be "sparry dolomite" fluid.

Sweetwater District

Crush analyses

Sphalerite. Gas compositions of Sweetwater sphalerite inclusion fluids (Table 3 and Fig. 8) are similar to Type I and Type II inclusion fluids in Mascot-Jefferson City sphalerite, with some important differences. On the H_2O-CH_4 binary (Fig. 8a), Sweetwater sphalerite fluids plot on the trend established by Mascot-Jefferson City sphalerite fluids (Fig. 4a), although the average CH_4 content is lower for Sweetwater sphalerite (1.2 mol% vs. 1.7 mol% at Mascot-Jefferson City). CO_2 values in Sweetwater sphalerite are commonly below 0.2 mol%, and essentially invariant (Fig. 8b), demonstrating no correlation with H_2O.

Other minor gas species are present in greater amounts at Sweetwater than at Mascot-Jefferson City. Argon averages 115 ppm (vs. 41 ppm at Mascot-Jefferson City), N_2 exceeds 0.1 mol% in three analyses, and total sulfur averages over 300 ppm (vs. <250 ppm at Mascot-Jefferson City). The H_2S/SO_2 ratio averages 2.17 for Sweetwater crushes, with sulfur gas species falling on a poor linear trend with a positive slope (Fig. 8c).

Fluorite. Results for Sweetwater fluorite samples that were analyzed by crushing are presented along with sphalerite data in Table 3 and Fig. 8. Fluorite inclusion fluids contain low amounts of CH_4 (averaging 0.78 mol%), CO_2 (0.17 mol%), and Ar (66 ppm) compared to sphalerite. On the H_2O-CH_4 binary (Fig. 8a), Sweetwater fluorite analyses fall directly on the sphalerite trend, but only on the lower CH_4 portion, with CH_4 values ranging from 0.5 to 1.3 mol%. CO_2 content does not vary much in the samples (Fig. 8b). Total sulfur gas content values average 636 ppm, with an average H_2S/SO_2 ratio of 4.58. Excepting one analysis, H_2S and SO_2 correlate linearly (Fig. 8c), but the best-fit line slope is only 0.14.

Barite. Of twelve crush analyses of Sweetwater barite (Table 3), only three yielded realistic gas compositions. The other samples have greatly elevated N_2, O_2, and Ar abundances, likely due to atmospheric contamination of the sample (possibly by entrapment of air along cleavage planes) prior to analysis. With one exception, N_2 contents in barite analyses are greater than 0.2 mol%, and two analyses yielded 66 mol% N_2.

The lack of N_2 in fluids from the other districts suggests that barite analyses with the lowest amount of N_2 are the best examples of the barite-forming fluid. Barite analyses with less than 0.6 mol% N_2 are similar to Sweetwater sphalerite with regard to CH_4 (1.03 mol%), CO_2 (0.11 mol%), and Ar (94 ppm). On the H_2O-CH_4 binary (Fig. 8a), these barite compositions plot near the linear trend established by Sweetwater sphalerite and fluorite, but CO_2 does not vary with H_2O (Fig. 8b). Sulfur gas content is much higher than in sphalerite and fluorite, averaging over 1000 ppm, and the

TABLE 2. FLUID INCLUSION COMPOSITIONS FROM BAKED MASCOT-JEFFERSON CITY CRUSH ANALYSES AND THERMAL DECREPITATION ANALYSES (MOLE PERCENT)

2A. CRUSH ANALYSES OF BAKED UNZONED SPHALERITE AND BAKED SPHALERITE CONTAINING PREDOMINANTLY ONE SPECIFIC INCLUSION TYPE

SAMPLE	H2O	CO2	CO	CH4	C2H6	C3H8	N2	Ar	H2S	SO2
UNZONED										
BC6SP1X	99.2	0.16	0.06	0.54	0.038	0.034	0.000	0.0054	0.0069	0.0064
BC6SP2X	99.0	0.22	0.05	0.66	0.033	0.039	0.000	0.0025	0.0067	0.0043
BC6SP3X	98.1	0.31	0.10	1.26	0.058	0.089	0.000	0.0053	0.0140	0.0090
BN96DS1X	98.0	0.27	0.16	1.13	0.000	0.347	0.000	0.0110	0.0230	0.0180
BN96DS2X	95.8	0.83	0.03	2.52	0.334	0.218	0.243	0.0081	0.0000	0.0000
BN96DS3X	98.3	0.46	0.00	0.60	0.099	0.128	0.409	0.0061	0.0000	0.0000
BY58R1X	96.2	0.69	0.26	2.60	0.047	0.119	0.000	0.0110	0.0260	0.0250
BY61R1X	97.3	0.56	0.15	1.76	0.072	0.041	0.000	0.0120	0.0190	0.0140
TYPE I										
BY32A1X	91.9	0.62	0.49	4.71	0.000	2.094	0.000	0.1000	0.0160	0.0160
BY9A1X	97.0	0.70	0.21	1.35	0.000	0.531	0.000	0.0310	0.0180	0.0230
BY9A2X	94.1	0.72	0.48	2.30	0.000	1.963	0.000	0.1410	0.0570	0.0870
TYPE II										
BY32V1X	93.4	0.33	0.32	3.63	0.000	2.119	0.000	0.1020	0.0160	0.0260
BY61V1X	98.0	0.89	0.12	0.86	0.041	0.035	0.000	0.0095	0.0130	0.0110
BY9V1X	91.3	6.43	0.09	1.63	0.185	0.224	0.000	0.0200	0.0150	0.0120
BY9V2X	97.7	0.30	0.18	1.23	0.000	0.511	0.000	0.0260	0.0200	0.0210
TYPE III										
BY61SA1X	91.1	4.36	0.27	3.92	0.251	0.061	0.000	0.0140	0.0220	0.0086
BY61SV1X	87.9	3.72	0.66	6.96	0.000	0.601	0.000	0.0230	0.0420	0.0084
BY61SV2X	97.8	0.99	0.13	0.95	0.070	0.055	0.000	0.0078	0.0110	0.0150
BY61SV3X	95.9	2.11	0.09	1.63	0.088	0.070	0.000	0.0089	0.0230	0.0170
BY61VS1X	96.9	1.39	0.11	1.44	0.075	0.033	0.000	0.0057	0.0230	0.0230
AVERAGE										
UNZONED	97.7	0.44	0.10	1.38	0.085	0.127	0.081	0.0077	0.0120	0.0096
TYPE I	94.3	0.68	0.39	2.79	0.000	1.529	0.000	0.0907	0.0303	0.0420
TYPE II	95.1	1.99	0.18	1.84	0.057	0.722	0.000	0.0394	0.0160	0.0175
TYPE III	93.9	2.51	0.25	2.98	0.097	0.164	0.000	0.0119	0.0242	0.0144

2B. CRUSH ANALYSES OF BAKED SPARRY DOLOMITE

SAMPLE	H2O	CO2	CO	CH4	C2H6	C3H8	N2	Ar	H2S	SO2
BC93D1X	94.7	3.58	0.11	1.45	0.029	0.031	0.000	0.0120	0.0120	0.0073
BC93D2X	94.1	4.24	0.12	1.36	0.021	0.038	0.000	0.0120	0.0150	0.0060
BI10D1X	98.3	0.96	0.04	0.64	0.023	0.016	0.000	0.0032	0.0077	0.0023
BI10D2X	95.0	2.44	0.09	2.27	0.040	0.043	0.000	0.0130	0.0250	0.0093
BN89D1X	98.6	0.46	0.09	0.81	0.000	0.022	0.000	0.0019	0.0071	0.0012
BN89D2X	98.5	0.71	0.06	0.62	0.007	0.021	0.000	0.0016	0.0100	0.0026
BY7D1X	96.3	2.02	0.12	1.40	0.041	0.033	0.000	0.0089	0.0130	0.0049
AVERAGE	96.5	2.06	0.09	1.22	0.023	0.029	0.000	0.0075	0.0128	0.0048

2C. INDIVIDUAL INCLUSION BURSTS FROM SPHALERITE THERMAL DECREPITATION ANALYSES

SAMPLE	H2O	CO2	CH4
N44DSP5A	99.3	0.36	0.29
N44DSP5C	98.3	0.22	1.46
N44DSP5E	95.8	0.95	3.23
N44LSP5A	99.2	0.19	0.57
N44LSP5B	99.2	0.27	0.49
I18LSP5A	98.7	0.06	1.24
I18LSP5B	97.7	1.47	0.80
C39SP5A	95.4	2.61	2.00
C39SP5B	93.8	3.53	2.65
C39SP5C	96.3	2.03	1.63
C39SP5E	99.2	0.58	0.27
C39SP5F	93.3	4.44	2.29
C39SP5G	95.8	2.26	1.95
C39SP5H	93.8	3.53	2.65
C39SP5I	91.1	5.02	3.83
C39SP6A	91.6	4.87	3.53
C39SP6B	92.4	4.91	2.73

FIRST LETTER OF SAMPLE NAME: C = COY MINE, I = IMMEL MINE, N = NEW MARKET MINE, Y = YOUNG MINE

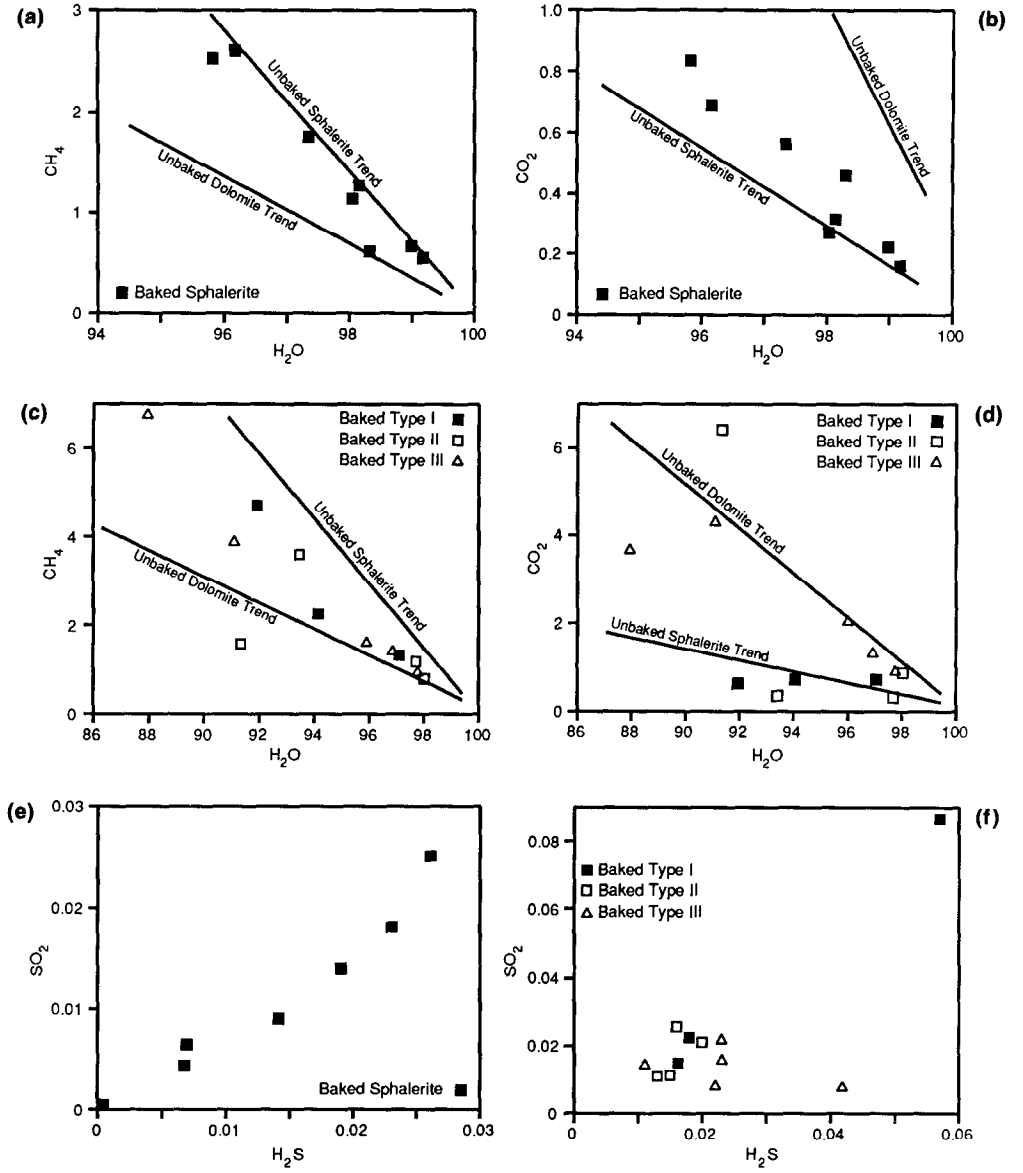

FIG. 5. H_2O-gas binary representations of baked MJC sphalerite. Trends of unbaked sphalerite and dolomite are shown as lines on some of the diagrams. (a) H_2O-CH_4, crush analyses. (b) H_2O-CO_2, crush analyses. (c) H_2O-CH_4, specific inclusion type crushes. (d) H_2O-CO_2, specific inclusion type crushes. (e) H_2S-SO_2, crush analyses. (f) H_2S-SO_2, specific inclusion type crushes.

H_2S/SO_2 ratio averages 3.0. On the H_2S-SO_2 binary (Fig. 8c), barite fluids plot closer to the sphalerite trend than to the fluorite trend.

Copper Ridge District

Crush analyses

Sphalerite. Sphalerite from several locations in the Copper Ridge district was analyzed by crushing (Table 4 and Fig. 9). Fluid compositions plot linearly on the H_2O-CH_4 binary (Fig. 9a), but, excepting two analyses, CH_4 values are less than 1.6 mol%. The H_2O-CO_2 binary shows more scatter (Fig. 9b), but there is still a general trend of increasing CO_2 with decreasing H_2O. CO_2 exceeds 0.4 mol% in only one analysis. Total sulfur averages 321 ppm (Fig. 9c), with an average H_2S/SO_2 ratio of 2.28 (excluding one anomalously high value). Seven of the sixteen analyses yielded N_2, with an average abundance of 174 ppm.

Sparry dolomite. Dolomite from Copper Ridge (Table 4) has elevated CO_2 values (0.5 to 1.1 mol%) and reduced CH_4 values (0.3 to 0.8) compared to sphalerite, and plots off the sphalerite trend on both the H_2O-CH_4 and H_2O-CO_2 binaries (Fig. 9a, b). Inclusion fluids average 98.5 mol% H_2O in the dolomite; nonaqueous gas components have fairly low abundances. N_2 was not detected in any of the analyses. Total sulfur averages 355 ppm, with an average H_2S/SO_2 ratio of 2.28. Dolomite and sphalerite gas compositions plot together on the H_2S/SO_2 binary (Fig. 9c).

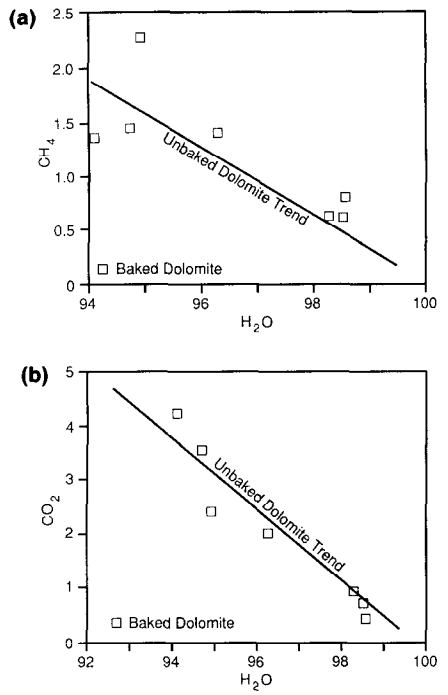

FIG. 6. H_2O-gas binary representations of baked MJC sparry dolomite. Trend of unbaked dolomite is shown as a line. (a) H_2O-CH_4. (b) H_2O-CO_2.

INTERPRETATION OF FLUID INCLUSION GAS ANALYSES

Comparison of Fluids Among Districts

Similarities in gas compositions obtained in this study suggest that these east Tennessee MVT districts could have been mineralized by the same or very similar solutions. In particular, sphalerite in all three districts, as well as fluorite in Sweetwater, share several characteristics.

At Mascot-Jefferson City, gas compositions from crush analyses of sphalerite with different colors and specific inclusion types all plot on the same linear trend on the H_2O-CH_4 binary, and in the same regions of the H_2O-CO_2 binary. The compositional range of dark sphalerite fluids on both binaries (Fig. 4c, d) is essentially the same as the range of Type I inclusion fluids (Fig. 4e, f). Similarly, light sphalerite compositions correspond to the range of Type II inclusion fluids (Fig. 4c–f). This suggests that these two inclusion types were associated with different episodes of sphalerite precipitation.

In contrast, similarities between Type III sphalerite inclusion compositions and sparry dolomite fluids substantiate the optical determination that Type III inclusions are related to deformed crystals and are likely secondary; they appear to contain fluid that was associated with dolomite deposition and was incorporated in some sphalerite as secondary inclusions. Baked Mascot-Jefferson City sphalerite compositions plot away from the unbaked sphalerite trends and toward the unbaked dolomite trends on both the H_2O-CH_4 and H_2O-CO_2 binaries (Fig. 5a, b). Analyses of baked samples with specific inclusion types show that it is probably the Type III inclusions that are responsible for this deviation (Fig. 5d). By inference, individual inclusion burst compositions that plot on the sparry dolomite trend were Type III inclusions. Baked sparry dolomite inclusion compositions are identical to unbaked compositions, suggesting there was not an additional secondary fluid in dolomite that could be separated by heating.

The CH_4 compositional trends of sphalerite fluids from both Sweetwater and Copper Ridge coincide with the trend established for Mascot-Jefferson City sphalerite (Figs. 8a and 9a), and sphalerite from all three districts has comparable H_2S and SO_2 values (Figs. 4g, 8c, and 9c). This suggests that the two fluids associated with sphalerite formation at Mascot-Jefferson City were also present during sphalerite formation in the other two districts. Sweetwater fluorite fluids also plot on the same CH_4 trends (Fig. 8a), but only in the CH_4-poor range corresponding to Type II Mascot-Jefferson City inclusions. Apparently fluorite precipitation did not take place while the Type I fluid was at Sweetwater. In contrast to CH_4, CO_2 abundances at both Sweetwater and Copper Ridge are lower than at Mascot-Jefferson City (Figs. 8b and 9b).

Mascot-Jefferson City and Copper Ridge sparry dolomite fluid compositions also show that one fluid may have been responsible for regional dolomite formation. Dolomite fluids from both districts plot on linear H_2O-CH_4 and H_2O-CO_2 trends that are distinct from the sphalerite/fluorite fluid trends (Fig. 9a, b), and both dolomite fluids have similar H_2S/SO_2 ratios (Figs. 4i and 9c).

To summarize, fluid inclusion gas compositions indicate that some fluids responsible for MVT mineralization in east Tennessee were present in all three districts studied. Mascot-Jefferson City sphalerite contains two fluids that were likely responsible for sphalerite precipitation in Type I and Type

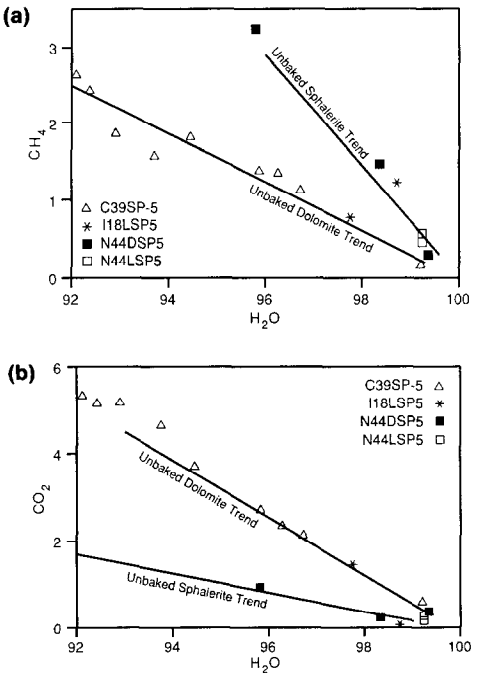

FIG. 7. H_2O-gas binary representations of individual bursts from Mascot-Jefferson City sphalerite. Trends of sphalerite and dolomite crush analyses are shown as lines. (a) H_2O-CH_4. (b) H_2O-CO_2.

TABLE 3. FLUID INCLUSION COMPOSITIONS FROM UNBAKED SWEETWATER CRUSH ANALYSES OF SPHALERITE, BARITE, AND FLUORITE (MOLE PERCENT)

SAMPLE	H2O	CO2	CO	CH4	C2H6	C3H8	N2	Ar	H2S	SO2
SPHALERITE										
S1084S1X	99.2	0.04	0.01	0.40	0.021	0.050	0.152	0.0076	0.0180	0.0160
S1084S2X	97.3	0.20	0.04	2.06	0.200	0.065	0.000	0.0092	0.0510	0.0190
S1207S1X	98.2	0.14	0.13	1.10	0.000	0.135	0.136	0.0100	0.0300	0.0110
S1207S2X	96.7	0.16	0.09	2.37	0.038	0.291	0.141	0.0180	0.0440	0.0140
SB1151X	98.0	0.22	0.10	1.32	0.000	0.328	0.000	0.0029	0.0120	0.0028
SB1152X	98.1	0.20	0.13	1.34	0.038	0.151	0.000	0.0110	0.0140	0.0083
SB1153X	97.7	0.21	0.13	1.58	0.043	0.258	0.000	0.0140	0.0170	0.0110
SB22A1X	98.9	0.19	0.08	0.59	0.082	0.067	0.000	0.0083	0.0190	0.0097
SB22A2X	98.9	0.21	0.08	0.64	0.041	0.069	0.000	0.0069	0.0170	0.0067
SB22A3X	98.7	0.19	0.09	0.86	0.056	0.077	0.000	0.0075	0.0180	0.0110
SB22B1X	98.2	0.21	0.13	1.17	0.000	0.228	0.000	0.0400	0.0150	0.0086
SB22B2X	98.6	0.17	0.11	0.99	0.000	0.123	0.000	0.0110	0.0150	0.0067
SB22B3X	98.1	0.16	0.12	1.31	0.000	0.265	0.000	0.0220	0.0140	0.0091
SB791X	97.8	0.15	0.11	1.60	0.143	0.153	0.000	0.0063	0.0130	0.0049
SB792X	98.6	0.16	0.06	0.99	0.092	0.075	0.000	0.0052	0.0120	0.0070
SB793X	98.2	0.17	0.08	1.25	0.130	0.097	0.000	0.0045	0.0190	0.0130
FLUORITE										
S1168F1X	99.1	0.11	0.13	0.49	0.000	0.032	0.000	0.0150	0.0360	0.0240
S1168F2X	99.1	0.16	0.09	0.46	0.020	0.024	0.000	0.0078	0.0430	0.0110
S1190F1X	98.9	0.10	0.09	0.77	0.007	0.034	0.000	0.0020	0.0360	0.0049
S1190F2X	98.0	0.24	0.19	1.30	0.000	0.082	0.000	0.0063	0.0650	0.0100
S1207F1X	99.2	0.08	0.08	0.51	0.000	0.029	0.000	0.0014	0.0300	0.0035
S1207F2X	98.2	0.30	0.13	1.14	0.028	0.034	0.000	0.0074	0.1030	0.0150
BARITE										
SW71B1X	57.3	1.76	0.00	19.75	0.952	0.547	3.189	0.5390	5.4350	2.0420
* SW71B2X	99.0	0.11	0.08	0.46	0.000	0.027	0.022	0.0062	0.0780	0.0200
* SW60B1X	97.1	0.10	0.00	1.72	0.000	0.117	0.530	0.0120	0.0900	0.0480
* SW60B2X	98.5	0.10	0.00	0.92	0.031	0.039	0.245	0.0100	0.0580	0.0180
SW106B1X	0.8	0.00	0.00	62.62	4.332	0.662	17.982	0.4800	0.0320	0.0740
SW106B2X	47.2	0.29	0.10	36.89	2.923	0.597	9.444	0.1900	0.0690	0.0710
SW79B1X	1.2	0.00	0.00	1.39	0.000	0.307	66.527	1.2890	0.1300	0.1100
SW79B2X	0.1	0.32	0.00	1.01	0.000	0.298	66.412	1.4460	0.1710	0.2080
SW72B1X	89.5	0.08	0.01	6.01	0.164	0.109	2.830	0.0640	0.0500	0.0380
SW72B2X	94.6	0.11	0.00	4.21	0.150	0.098	0.608	0.0110	0.0330	0.0120
AVERAGE										
SPHALERITE	98.2	0.17	0.09	1.22	0.055	0.152	0.027	0.0115	0.0205	0.0099
FLUORITE	98.8	0.17	0.12	0.78	0.009	0.039	0.000	0.0066	0.0522	0.0114
BARITE(*)	98.2	0.11	0.03	1.03	0.010	0.061	0.266	0.0094	0.0753	0.0287

* = BARITE ANALYSES USED TO DETERMINE THE AVERAGE FLUID COMPOSITION

II inclusions. Both fluids may also have been responsible for sphalerite precipitation at Sweetwater and Copper Ridge. The Type II sphalerite inclusion fluid appears to have been present in fluorite at Sweetwater. The similarities among fluids in the different districts imply that mineralization in east Tennessee formed as part of a regional event, rather than as separate but similar events.

Gas Solubilities and Trapping Pressures

Most sphalerite inclusion fluids analyzed in this study contain large amounts of volatiles, especially CH_4 (0.3 to 2.9 mol%) and CO_2 (0.1 to 1.0 mol%). At temperatures of 100 to 200°C, the brines would have required high pressure to keep that much gas in solution (HAAS, 1978; HANOR, 1980). Saturation pressures calculated for the appropriate fluid temperature and salinity using SOLMINEQ.88 (KHARAKA et al., 1988) for Mascot-Jefferson City sphalerite compositions range from 200 to 300 bars (depending on fluid temperature) for the gas-poor inclusion compositions, to as much as 2200 bars for the gas-rich inclusion compositions. These gas-rich compositions would require burial depths of more than 6 km even under lithostatic pressure (as much as 20 km under hydrostatic pressure), whereas the gas-poor compositions require burial depths of less than a kilometer under lithostatic pressure (2 to 3 km under hydrostatic pressure). Although it is difficult to be certain of the depth of mineralization for most MVT districts, the Upper Knox in east Tennessee and Virginia is estimated to have been buried to a depth of 2 to 3 km (GROVER and READ, 1983) during Devonian time, the age of mineralization obtained by NAKAI et al. (1990). At that depth the gas-poor compositions could have existed in solution, but the gas-rich compositions could not have existed as one phase even under lithostatic pressure.

Location of a Vapor Phase in Samples

Information presented in the previous section indicates that our gas-rich fluid inclusion analyses represent either mixtures of separate liquid-rich and vapor-rich inclusions, or liquid-rich inclusions with excess vapor (two-phase trapping). Vapor inclusions have not been positively identified in Mascot-Jefferson City sphalerite. HAYNES et al. (1989) suggested that Type II inclusions might be vapor-rich, but the quadrupole analyses presented here, as well as crushing stage tests, suggest they are aqueous. Additionally, individual bursts observed in quadrupole thermal decrepitation runs yield compositions that plot along the linear trends on binary

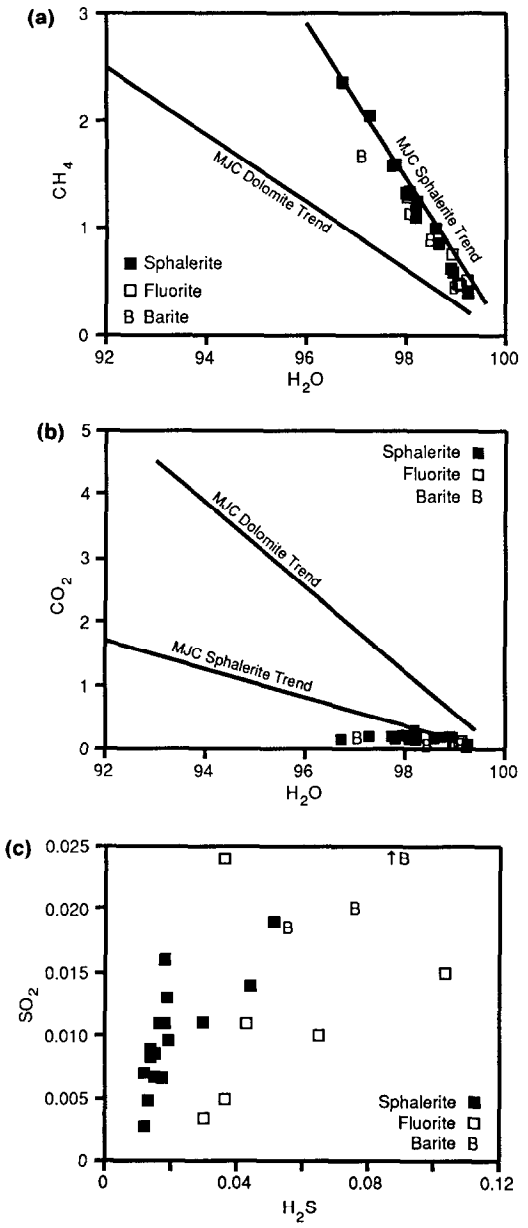

FIG. 8. H_2O-gas binary representations of Sweetwater sphalerite, fluorite, and barite crush analyses. Mascot-Jefferson City sphalerite and dolomite trends are shown as lines. Only three barite analyses are included. (a) H_2O-CH_4. (b) H_2O-CO_2. (c) H_2S-SO_2.

diagrams established by crushing analyses (Fig. 7). If discrete endmember fluids resided in separate inclusions, individual burst compositions should plot either at the gas-poor end of the mixing lines, or as pure vapors. Yet some individual bursts have compositions with CH_4 values too great to have existed in aqueous solution.

It is possible that individual bursts that we monitor are not from individual inclusions. A mixed-member composition could also result if decrepitating aqueous inclusions simultaneously ruptured neighboring vapor inclusions. However, for bursts that occur above 400°C, the temperature at which resolvable bursts began to be noted in most runs, there is a correlation between decrepitation temperature and composition, with gas-rich bursts occurring at higher temperatures (Fig. 10). This suggests that the vapor component is present in the same inclusions as the aqueous component. Inclusions with less vapor would attain internal pressures necessary for decrepitation at lower temperatures than gas-rich inclusions.

The behavior of secondary "dolomite fluid" inclusions in sphalerite provides additional evidence against vapor-rich inclusions as the source of the analyzed vapor phase. Individual bursts from some sphalerite samples yield compositions that plot directly on the H_2O-CH_4 and H_2O-CO_2 trends established by Mascot-Jefferson City sparry dolomite. More significant, though, is the observation that sample I18LSP-5, and possibly sample N44DSP5, had individual burst compositions that plot on both the sphalerite and dolomite binary trends. This is likely to occur only if the bursts are actually individual inclusions; with two types of inclusion fluids available, compositions would plot somewhere between the dolomite and sphalerite trends if multiple inclusions released their fluids simultaneously. Thus, high-CH_4 contents in some individual bursts are likely due to excess vapor coexisting along with the aqueous component in single inclusions.

Geologic Significance of Binary H_2O-Gas Trends

If the linear H_2O-CH_4 and H_2O-CO_2 trends are due to actual compositional variation, as we believe (see Experimental Procedure section), and not entirely created by varying degrees of adsorption of H_2O during analysis, extrapolation of the trends to 0 mol% H_2O can be used to crudely estimate CH_4 and CO_2 mole percentages in the coexisting vapor phase associated with the mineralizing fluids. Zero-H_2O intercepts can also be determined from best-fit lines on other H_2O-gas binaries, resulting in a complete vapor phase composition associated with each mineral (Table 5). Vapor phase compositions estimated in this manner for sphalerite in all three districts, as well as for fluorite at Sweetwater, are CH_4-rich, whereas inferred sparry dolomite vapor phases at Mascot-Jefferson City and Copper Ridge are CO_2-dominated. Ethane and propane also account for several mol% in the sphalerite- and fluorite-associated vapor phases. H_2S makes up less than 1 mol% of the inferred sphalerite vapor phase at Mascot-Jefferson City and Copper Ridge, but 4.5 mol% in the Sweetwater fluorite vapor phase.

These vapor phases might have formed by phase separation (boiling) from the Type I and Type II sphalerite aqueous solutions. Phase separation could have occurred if the aqueous solution was initially overpressured, as has been postulated previously for the region (HAYNES et al., 1989). The presence of shale units and an inferred rapid sedimentation rate for the Sevier basin (SHANMUGAN and WALKER, 1980) could have resulted in fluid pressures in excess of hydrostatic values, and local pockets of overpressured carbonates may have existed in east Tennessee (HAYNES et al., 1989). Under such conditions, mineralizing fluids would have dissolved more gas than they could retain under hydrostatic pressure. Subsequent reduction to hydrostatic pressure by fracturing of overlying rock, or emergence from beneath an aquiclude, would result in exsolution of a vapor phase (HANOR, 1988), which could then be trapped in varying amounts with the new reduced-pressure aqueous component to produce the observed linear compositional trends.

TABLE 4. FLUID INCLUSION COMPOSITIONS FROM UNBAKED COPPER RIDGE CRUSH ANALYSES OF SPARRY DOLOMITE AND SPHALERITE (MOLE PERCENT)

SAMPLE	H2O	CO2	CO	CH4	C2H6	C3H8	N2	Ar	H2S	SO2
DOLOMITE										
CRD1X	98.4	0.51	0.12	0.78	0.029	0.025	0.000	0.0057	0.0240	0.0140
CRD2X	99.0	0.47	0.04	0.41	0.004	0.022	0.000	0.0026	0.0220	0.0073
IDD1X	98.0	1.08	0.10	0.65	0.007	0.030	0.000	0.0024	0.0290	0.0150
IDD2X	98.7	0.83	0.04	0.34	0.000	0.031	0.000	0.0019	0.0220	0.0089
SPHALERITE										
CRS1X	99.0	0.18	0.06	0.58	0.022	0.033	0.011	0.0069	0.0230	0.0120
CRS2X	99.6	0.07	0.01	0.18	0.003	0.018	0.045	0.0015	0.0120	0.0039
E486S1X	99.0	0.06	0.04	0.70	0.020	0.024	0.056	0.0021	0.0070	0.0100
E486S2X	99.0	0.13	0.06	0.66	0.014	0.030	0.000	0.0031	0.0130	0.0050
E511S1X	97.8	0.18	0.21	1.52	0.000	0.167	0.000	0.0087	0.0160	0.0110
E511S2X	93.4	0.56	0.44	4.67	0.171	0.397	0.000	0.0240	0.0690	0.0380
ID860S1X	97.3	0.23	0.01	1.95	0.243	0.106	0.020	0.0100	0.0180	0.0140
ID860S2X	98.3	0.35	0.18	0.96	0.000	0.095	0.000	0.0072	0.0290	0.0140
IDS2X	98.2	0.38	0.11	1.09	0.000	0.106	0.000	0.0072	0.0290	0.0240
R261S1X	99.2	0.09	0.06	0.55	0.019	0.051	0.000	0.0033	0.0110	0.0042
R261S2X	99.2	0.10	0.06	0.49	0.010	0.051	0.000	0.0040	0.0180	0.0058
W325S1X	99.2	0.03	0.04	0.62	0.022	0.035	0.000	0.0022	0.0280	0.0029
W325S2X	99.1	0.08	0.04	0.62	0.011	0.031	0.048	0.0027	0.0200	0.0047
W326S1X	98.9	0.09	0.05	0.75	0.028	0.076	0.000	0.0038	0.0160	0.0048
W326S2X	98.5	0.11	0.04	1.08	0.034	0.093	0.081	0.0052	0.0130	0.0054
AVERAGE										
DOLOMITE	98.5	0.72	0.08	0.54	0.010	0.027	0.000	0.00315	0.02425	0.0113
SPHALERITE	98.4	0.18	0.09	1.09	0.040	0.088	0.017	0.00613	0.02147	0.01064

LOCATIONS
FIRST LETTER OF SAMPLE NAME: C = UNSPECIFIED, E = EIDSON, I = IDOL MINE, R = SHILOH, W = BIG WAR CREEK

Alternatively, the vapor could represent a pre-existing gas phase that was encountered by the aqueous fluid. CH_4 and other gases could have been incorporated from a gas cap and retained in the fluid as small bubbles. Although natural gas compositions vary widely, the inferred vapor compositions associated with sphalerite in this study are similar to an analysis of natural gas from the Smackover formation in Florida (COLLINS, 1974), which contained 86.5 mol% total alkanes (69.2 mol% CH_4), 7.2 mol% H_2S, and 3.3 mol% CO_2. Bitumen from mature oil is present in Mascot-Jefferson City sphalerite, although we have not seen evidence for liquid hydrocarbons in inclusions from either UV fluorescence (KETTLER, 1990) or CH_4-to-higher alkane ratios in quadrupole analyses.

The vapor associated with sphalerite at Mascot-Jefferson City had a different composition than the vapor associated with gangue sparry dolomite. This might imply that reduction of pressure is more likely to have been the cause of the vapor phase than a previously-existing localized gas cap, and that the vapor is genetically related to the mineralizing fluid. Otherwise, the vapor would have the same composition in any mineral at the site. The occurrence of similar vapor compositions associated with sphalerite mineralization in all three districts is also evidence for gas unmixing from one regional mineralizing fluid, rather than incorporation of pre-existing gas at each district. However, it is possible that a gas cap was present and that phase separation associated with sparry dolomite precipitation (LEACH et al., 1991) added CO_2 to the vapor from the gas cap, effectively diluting the amount of CH_4 incorporated into sparry dolomite inclusions.

Effect of Vapor Component on Inclusion Filling Temperatures

Homogenization of a fluid inclusion to the liquid phase occurs where the isochore for the fluid intersects the bubble-point curve for that fluid composition. For any specific isochore with a positive slope, homogenization of a gas-rich inclusion will occur at a higher temperature than for a pure water inclusion.

The effect of trapped vapor on fluid inclusion filling temperatures typical of the east Tennessee MVT deposits is shown in Fig. 11, where calculated bubble-point curves for the gas-poor and gas-rich endmember inclusion compositions from sphalerite are plotted on a *P-T* diagram. Also included in the figure are calculated isochores for the Type I inclusion aqueous endmember gas composition at three different densities (the isochores calculated for the Type II inclusion aqueous endmember plot almost on top of the Type I isochores). The intersections of one of these isochores with the bubble-point curves indicate the lowest and highest filling temperatures that should be observed in a fluid of given density for our reported range of compositions. Thus, varying amounts of vapor trapped along with an aqueous component in inclusions should produce a range of homogenization temperatures. These isochores were calculated for fluids of 0% salinity; addition of salt to the solutions at temperatures less than 300°C causes the isochore slopes to decrease (SOURIRAJAN and KENNEDY, 1962; ROEDDER and BODNAR, 1980; ZHANG and FRANTZ, 1987), providing an even larger homogenization temperature range.

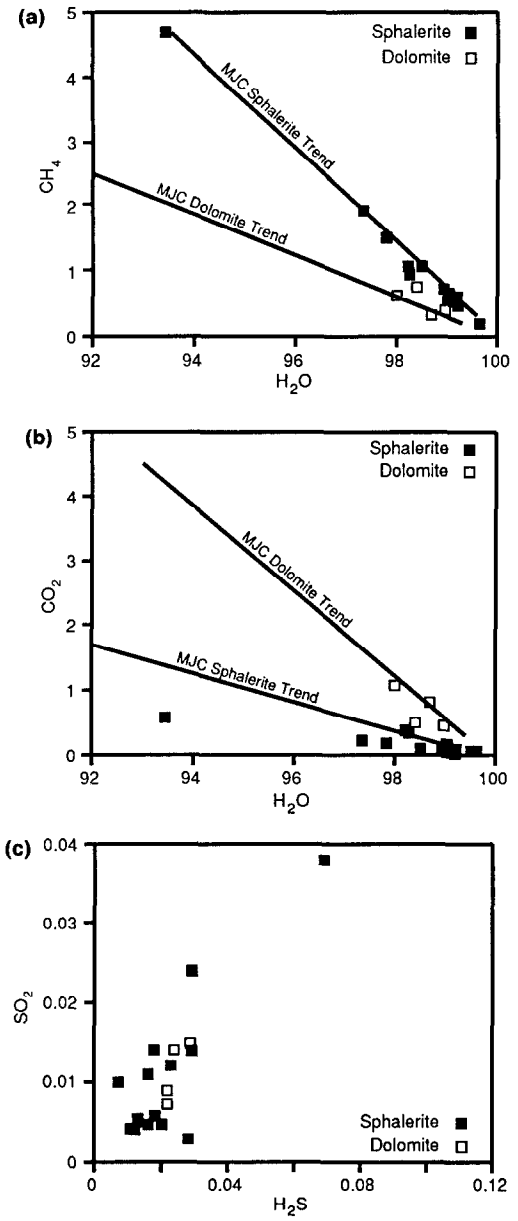

FIG. 9. H_2O-gas binary representations of Copper Ridge sphalerite and sparry dolomite crush analyses. MJC sphalerite and dolomite trends are shown as lines. (a) H_2O-CH_4. (b) H_2O-CO_2. (c) H_2S-SO_2.

The observed range of fluid compositions detected by the quadrupole analyses could be produced by (varying) small amounts of vapor incorporated into individual inclusions along with the aqueous fluid. Differences in the amount of each phase that are large enough to alter inclusion filling temperatures by tens of degrees may not be visually observable. HAYNES et al. (1989) showed that the inclusion freezing point temperatures of Mascot-Jefferson City sphalerite reported by TAYLOR et al. (1983) appear to have a trimodal distribution. Yet each salinity range defined by HAYNES et al. (1989) corresponds to a wide homogenization temperature range, with some temperatures higher than are commonly observed in MVT deposits (ROEDDER, 1967; Fig. 12). Additionally, TAYLOR et al. (1983, their Fig. 6) reported ranges of several tens of degrees in homogenization temperatures for samples that had almost invariant freezing temperatures. This range of homogenization temperatures reported in previous studies may in itself be evidence for initial incorporation of varying proportions of vapor and liquid phases into individual inclusions. From Fig. 11, an isochore for a fluid density of 0.91 or 0.92 could account for the range of filling temperatures observed in fluid inclusions in sphalerite in east Tennessee.

Homogenization of the gas-rich inclusions could occur only at high internal pressures, perhaps in excess of a kilobar. Survival of inclusions to such high internal pressures may seem unlikely, but our thermal decrepitation runs indicate that many inclusions survive heating to well above 400°C before decrepitating. From the isochores in Fig. 11, this must represent a high internal pressure regardless of where the bubble-point curve lies. Extrapolation of the BODNAR and BETHKE (1984) sphalerite stretching data down to the smaller inclusion sizes typical in Mascot-Jefferson City sphalerite suggests that the gas-rich inclusions may stretch before homogenizing, but sphalerite decrepitation behavior is less well characterized. The thermal decrepitation runs indicate that the gas-rich inclusions can survive high enough internal pressures to homogenize before decrepitating.

Implications for MVT Depositional Mechanisms

The apparent coexistence of mineralizing brines with a vapor phase in the east Tennessee districts has important ramifications for possible depositional mechanisms for sulfides and gangue dolomite. The vapor could have caused minerals to deposit from the associated brine in two ways.

The first method is by partitioning of gases such as CO_2 and H_2S from the liquid into the vapor. This effect would occur regardless of whether the vapor formed by actual separation from the brine or was a pre-existing natural gas accumulation that mixed with the brine. Among the most important results of this vapor separation would be an increase in pH of the solution (DRUMMOND and OHMOTO, 1985), which would cause deposition of both carbonate and sulfide

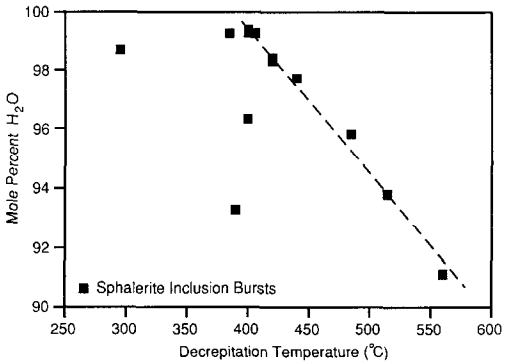

FIG. 10. Water content vs. decrepitation temperature for sphalerite individual inclusion bursts. Note the apparent linear relation above 400°C. Few individual bursts from sphalerite are recognizable below 400°C during thermal decrepitation runs.

TABLE 5. INFERRED MOLE PERCENT COMPOSITIONS OF VAPOR PHASES ASSOCIATED WITH EAST TENNESSEE MINERALIZATION (DETERMINED BY EXTRAPOLATING FLUID INCLUSION COMPOSITIONAL TRENDS TO ZERO H2O)

5A. SPHALERITE AND FLUORITE

	MASCOT-JEFFERSON CITY SPHALERITE----------						COPPER RIDGE	SWEETWATER	
	ALL	DARK	LIGHT	TYPE I	TYPE II	TYPE III	SPH	SPH	FLT
CO2	10.4	1.6	27.0	3.9	16.5	9.3	8.4	2.1	14.8
CO	2.7	0.0	5.7	1.6	0.0	4.7	6.5	1.7	6.6
CH4	74.6	81.2	59.6	79.8	44.9	76.7	71.7	80.2	68.0
ETHANE	4.6	6.9	0.9	6.2	4.7	4.9	3.1	2.4	0.6
PROPANE	4.4	10.7	4.2	4.3	6.8	2.3	6.1	8.7	3.0
N2	1.4	0.2	0.0	2.0	26.4	0.0	0.0	0.8	0.0
Ar	0.2	0.3	0.1	0.1	0.5	0.3	0.4	0.3	0.0
H2S	0.4	0.0	0.8	0.4	0.7	0.4	0.9	1.1	4.5
SO2	0.2	0.0	0.4	0.3	0.6	0.1	0.6	0.2	0.2
TOTAL	98.8	100.9	98.7	98.6	101.1	98.8	97.7	97.6	97.8
TOTAL ALKANES	83.6	98.8	64.7	90.2	56.5	84.0	81.0	91.3	71.7

5B. SPARRY DOLOMITE

	MJC	COPPER RIDGE
CO2	65.3	49.8
CO	0.1	7.6
CH4	32.7	33.1
ETHANE	0.4	0.9
PROPANE	0.4	0.6
N2	0.0	0.0
Ar	0.1	0.1
H2S	0.3	0.7
SO2	0.2	0.9
TOTAL	99.4	93.8
TOTAL ALKANES	33.5	34.6

minerals. Although this process would deposit sulfide minerals, including sphalerite (HAYNES et al., 1989), preliminary reaction-path calculations show that the ratio of dolomite gangue to sphalerite would be too high to produce ore-grade precipitates (LEACH et al., 1991).

The second way in which the vapor might cause mineral deposition would be by reaction with the liquid. Two such reactions can be envisioned. First, and least likely, the CH_4-rich vapor might react with dissolved SO_4^{2-} in the brine to produce H_2S and CO_2 (ANDERSON and GARVEN, 1987). As these authors point out, thermochemical sulfate reduction of this type is relatively common in some basinal settings. However, this process would be expected to yield isotopically light carbon, and sulfur with a range of isotopic compositions, neither of which are observed in the east Tennessee ores (HAYNES, 1986; JONES et al., 1990). On the other hand, any H_2S in the gas accumulation would react directly with the brine to produce metal sulfides. For a brine containing dissolved zinc, this mixing would cause large amounts of sphalerite to deposit, regardless of whether or not the brine contained any dissolved sulfur (HAYNES et al., 1989). Our extrapolated gas composition for the east Tennessee sphalerites contains about 0.5 mol% H_2S. Interestingly, mass balance calculations suggest that a 10-m-thick gas field measuring about 23 km on a side and with about 20% porosity would contain enough H_2S to form the sphalerite in the Mascot-

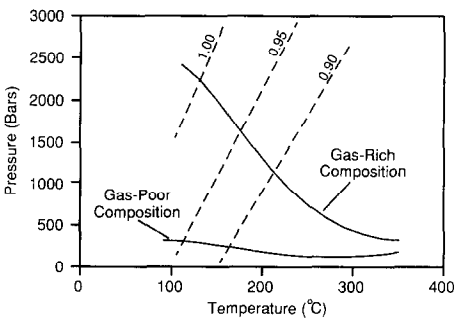

FIG. 11. Effect of trapped vapor component on fluid inclusion filling temperature. Bubble-point curves for the gas-rich and gas-poor compositions were calculated with SOLMINEQ.88 (KHARAKA et al., 1988) for appropriate salinity. Isochores for three different fluid densities are shown (calculated with FLINCOR, BROWN, 1988, using the Holloway soup equation of state option, HOLLOWAY, 1981). A given isochore will intersect intermediate composition bubble-point curves over a range of temperature, corresponding to a range of observed fluid inclusion filling temperatures.

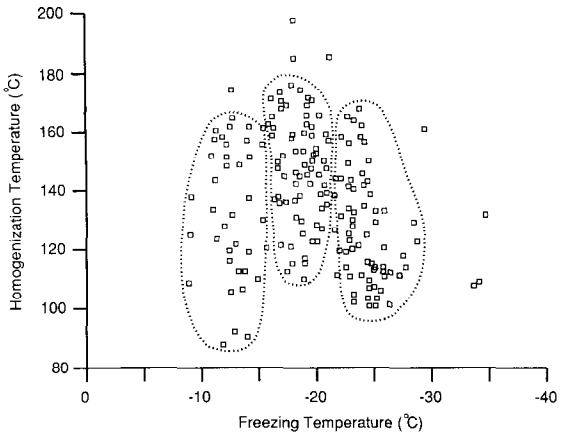

FIG. 12. Summary of sphalerite homogenization temperatures and freezing temperatures from the Mascot-Jefferson City district, showing the three salinity populations distinguished by HAYNES et al. (1989). Data are compiled from TAYLOR et al. (1983) and ZIMMERMAN and KESLER (1981). The three salinity populations distinguished by HAYNES et al. (1989) are outlined by the dotted lines.

Jefferson City district. This field would be about the same size as the district.

The inferred vapor compositions associated with sphalerite and fluorite at Sweetwater are also CH_4-rich and could also be related to a gas cap at that site. However, there is very little sphalerite at Sweetwater, and the inferred vapor with fluorite contains almost 10 times as much H_2S as the vapor with sphalerite at Mascot-Jefferson City. A gas cap at Sweetwater could simply have had more initial H_2S than gas caps at the other districts, but if the same Zn-rich fluid that invaded the other two districts encountered a gas cap at Sweetwater, there would have been a similar amount of sphalerite precipitated. Instead, it may be that some of the excess H_2S associated with Sweetwater fluorite was delivered in solution and added to any H_2S that may already have been present in a gas cap at that site. The H_2S-bearing brine would have been able to carry less dissolved Zn, resulting in less sphalerite at Sweetwater than in the other two districts. Although there are similarities among the brines in all three districts, we postulate that the mineralizing brine at Sweetwater incorporated an additional fluid component (H_2S-rich) that was not added to the fluids that reached Mascot-Jefferson City and Copper Ridge. This is not unreasonable, as there is already evidence for large amounts of barium and fluorine in the Sweetwater system that were apparently not present at the other two districts.

Although much of this model requires more evaluation, its appeal is that it provides a potential method to deposit sphalerite in specific locations within otherwise similar dolomitized breccia terranes. While dolomite and small amounts of sphalerite could have been deposited widely throughout east Tennessee by loss of the CO_2-rich vapor phase that we observe in the sparry dolomite analyses, locally massive sphalerite deposition would occur in response to mixing with a sour gas accumulation, such as indicated by our analyses of gases in sphalerite. The possibility that such gas traps were present during the probable Acadian mineralization event is indicated by HAYNES and KESLER (1989), who have shown that hydrocarbon accumulations in east Tennessee formed prior to Alleghenian (Pennsylvanian-Permian) time.

CONCLUSIONS

1) Similarities in inclusion gas compositions in the three districts indicate that MVT-mineralization in east Tennessee likely occurred as a regional event, rather than from separate fluids associated with each district. Sphalerite fluids in all three districts, as well as fluorite from the Sweetwater district, have similar H_2O-CH_4-CO_2 ratios. Sparry dolomite fluid compositions are the same in the Mascot-Jefferson City and Copper Ridge districts, but differ markedly from sphalerite fluids.
2) At Mascot-Jefferson City, CO_2-rich secondary fluids were incorporated into some sphalerite as Type III inclusions. The gas chemistry of this fluid is similar to that of apparently primary fluid in sparry dolomite.
3) The high gas contents of many inclusions require that a vapor phase was present along with the aqueous fluid in the analyzed samples. Calculated homogenization behavior and thermal decrepitation analyses indicate that the vapor phase was trapped in varying (small) amounts along with the aqueous phase in individual inclusions. The source of the vapor could be either from phase separation due to reduction of fluid pressure of over-pressured brines, or a pre-existing gas cap at mineralized sites.
4) The effect of varying amounts of CH_4-dominated vapor trapped along with aqueous fluid in sphalerite inclusions should be to provide a range of observed filling temperatures. For the range of gas compositions observed in this study, a fluid of density 0.91–0.93 could account for the temperature ranges previously reported for sphalerite in the region. Varying vapor/aqueous component ratios that are too small to notice visually may be responsible for large ranges of observed inclusion filling temperatures.
5) The presence of a vapor phase associated with the mineralizing brines may be directly related to sulfide deposition. If a vapor formed by phase separation from the brine, precipitated sparry dolomite:sphalerite ratios would probably be too high to result in an economic concentration of sphalerite. However, if the vapor source was a sour gas cap that was contacted by a Zn-rich fluid, high-grade sulfide zones could form within areas originally occupied by the gas cap.

Acknowledgments—We would like to thank Vance Greene and Frank Rasnick from ASARCO for tours and access to mines in the Mascot-Jefferson City district and for providing us with some samples. Allen Heyl of the USGS in Denver provided samples from many locations as well as very helpful information on Appalachian MVT mineralization. Gary Landis of the USGS was equally helpful in providing information on general principles of quadrupole analysis. David Norman supplied us with the "standard" HF-1, which was used to compare our analytical results to those of his laboratory. Parts of this research were supported by PRF grant #21478-AC2 from the American Chemical Society.

Editorial handling: T. C. Spooner

REFERENCES

ALEXANDROVSKA E. S., BANNIKOVA L. A., and SUSHCHEVSKAYA T. M. (1980) Errors in gas analysis in thermal expansion of inclusions. *Geochem. Intl.* **17**, 66–71.

ANDERSON G. M. and GARVEN G. (1987) Sulfate-sulfide-carbonate associations in Mississippi Valley-type lead-zinc deposits. *Econ. Geol.* **82,** 482–488.

BODNAR R. J. and BETHKE P. M. (1984) Systematics of stretching of fluid inclusions: I. Fluorite and sphalerite at 1 atmosphere confining pressure. *Econ. Geol.* **79,** 141–161.

BOURCIER W. L. (1986) A computer program for calculation of fluid inclusion phase equilibria in the system H_2O-NaCl-CO_2-CH_4-H_2S with applications to Mississippi Valley-type ore deposits (abstr.). *Eos* **67,** 1258.

BROWN P. E. (1988) *FLINCOR.* Wisc-Ware, Univ. Wisconsin-Madison.

CALESS J. A. (1983) Geology, paragenesis, and geochemistry of sphalerite mineralization at the Young mine, Mascot-Jefferson City district, east Tennessee. M.Sc. thesis, Virginia Polytechnic Inst. and State Univ.

COLLINS A. G. (1974) Geochemistry of liquids, gases, and rocks from the Smackover formation. *US Dept. of the Interior Rept. of Inv. No. 7897.*

CRAWFORD J. and HOAGLAND A. D. (1968) The Mascot-Jefferson City zinc district. In *Ore Deposits of the United States, 1933–1967 (Graton-Sales Volume)* (ed. J. D. RIDGE), pp. 242–256. AIME Inc.

DRUMMOND S. E. and OHMOTO H. (1985) Chemical evolution and mineral deposition in boiling hydrothermal systems. *Econ. Geol.* **80,** 126–147.

EBERS M. L. and KOPP O. C. (1979) Cathodoluminescent microstratigraphy in gangue dolomite, the Mascot-Jefferson City district, Tennessee. *Econ. Geol.* **74,** 908–918.

GARRETT R. G. (1969) The determination of sampling and analytical errors in exploration geochemistry. *Econ. Geol.* **64,** 568–574.

GROVER G., JR. and READ J. F. (1983) Paleoaquifer and deep burial related cements defined by regional cathodoluminescent patterns, Middle Ordovician carbonates, Virginia. *AAPG Bull.* **67,** 1275–1303.

HAAS J. L., JR. (1978) An empirical equation with tables of smoothed solubilities of methane in water and aqueous sodium chloride solutions up to 25 weight percent, 360°C, and 138 MPa. *USGS Open-file Rept. No. 78-1004.*

HANOR J. S. (1980) Dissolved methane in sedimentary brines: Potential effect on the PVT properties of fluid inclusions. *Econ. Geol.* **75,** 603–617.

HANOR J. S. (1988) Origin and migration of subsurface sedimentary brines. *SEPM Short Course No. 21.*

HAYNES F. M. (1986) Geologic and geochemical controls for sphalerite mineralization, Mascot-Jefferson City zinc district, east Tennessee. Ph.D. dissertation, University of Michigan.

HAYNES F. M. and KESLER S. E. (1989) Pre-Alleghenian (Pennsylvanian-Permian) hydrocarbon emplacement along Ordovician Knox unconformity, eastern Tennessee. *AAPG Bull.* **73,** 289–297.

HAYNES F. M., BEANE R. E., and KESLER S. E. (1989) Simultaneous transport of metal and reduced sulfur, Mascot-Jefferson City zinc district, east Tennessee: Evidence from fluid inclusions. *Amer. J. Sci.* **289,** 994–1038.

HEARN P. P. and SUTTER J. F. (1985) Authigenic potassium feldspar in Cambrian carbonates: Evidence of Alleghenian brine migration. *Science* **228,** 1529–1531.

HOAGLAND A. D. (1976) Appalachian zinc-lead deposits. In *Handbook of Stratabound and Stratiform Ore Deposits,* Vol. 6 (ed. K. H. WOLFE), pp. 495–534. Elsevier.

HOFSTRA A. H., LEACH D. L., LANDIS G. P., VIETS J. G., ROWAN E. L., and PLUMLEE G. S. (1989) Fluid inclusion gas geochemistry as a monitor of ore depositional processes in Mississippi Valley-type deposits in the Ozark region. In *US Geological Survey-Missouri Geological Survey Symposium: Mineral Resource Potential of the Midcontinent; USGS Open-File Rept. 89-169* (ed. W. P. PRATT and M. B. GOLDHABER), pp. 13–15.

HOLLOWAY J. R. (1981) Compositions and volumes of supercritical fluids in the earth's crust. In *MAC Short Course in Fluid Inclusions* (ed. L. S. HOLLISTER and M. L. CRAWFORD), Vol. 6, pp. 13–38. Mineral. Assoc. Can.

JONES H. D., KESLER S. E., and ALT J. C. (1990) Sulfur isotopes in central Appalachian MVT mineralization (abstr.). *Geol. Soc. Amer. 1990 Ann. Meet. Abstr. Prog.,* p. A222.

KESLER S. E., JONES L. M., and RUIZ J. (1988) Strontium isotopic geochemistry of Mississippi Valley-type deposits, east Tennessee: Implications for age and source of mineralizing brines. *Geol. Soc. Amer. Bull.* **100,** 1300–1307.

KETTLER R. M. (1990) Organic matter in hydrothermal systems: Implications for fluid chemistry and source. Ph.D. dissertation, University of Michigan.

KHARAKA Y. K., GUNTER W. D., AGGARWAL P. K., PERKINS E. H., and DEBRAAL J. D. (1988) SOLMINEQ.88: A computer program for geochemical modeling of water-rock interactions. *USGS Water-Res. Inv. Rep. 88-4227.*

LEACH D. L., PLUMLEE G. S., HOFSTRA A. H., LANDIS G. P., ROWAN E. L., and VIETS J. G. (1991) Origin of late dolomite cement by CO_2-saturated deep basin brines: Evidence from the Ozark region, central United States. *Geology* **19,** 348–351.

MCCORMICK J. E., EVANS L. L., PALMER R. A., and RASNICK F. D. (1971) Environment of the zinc deposits of the Mascot-Jefferson City district, Tennessee. *Econ. Geol.* **66,** 757–762.

NAKAI S., HALLIDAY A. N., KESLER S. E., and JONES H. D. (1990) Rb-Sr dating of sphalerites from Tennessee and the genesis of Mississippi Valley type ore deposits. *Nature* **346,** 354–357.

NORMAN D. I. and SAWKINS F. J. (1987) Analysis of volatiles in fluid inclusions by mass spectrometry. *Chem. Geol.* **61,** 1–10.

NORMAN D. I., TING W., PUTNAM B. R., and SMITH R. W. (1985) Mineralization of the Hansonburg Mississippi Valley-type deposit, New Mexico: Insight from the composition of gases in fluid inclusions. *Canadian Mineral.* **23,** 353–368.

ROEDDER E. (1967) Environment of deposition of stratiform (Mississippi Valley-type) ore deposits, from studies of fluid inclusions. *Econ. Geol. Mono.* **3,** 349–362.

ROEDDER E. (1971) Fluid inclusion evidence on the environment of formation of mineral deposits of the southern Appalachians. *Econ. Geol.* **66,** 777–791.

ROEDDER E. and BODNAR R. J. (1980) Geologic pressure determinations from fluid inclusion studies. *Ann. Rev. Earth Planet. Sci.* **8,** 263–301.

SHANMUGAN G. and WALKER K. R. (1980) Sedimentation, subsidence, and evolution of a foredeep basin in the Middle Ordovician, southern Appalachians. *Amer. J. Sci.* **280,** 479–496.

SOURIRAJAN S. and KENNEDY G. C. (1962) The system H_2O-NaCl at elevated temperatures and pressures. *Amer. J. Sci.* **260,** 115–141.

TAYLOR M., KESLER S. E., and CLOKE P. L. (1983) Fluid inclusion evidence for fluid mixing, Mascot-Jefferson City zinc district, Tennessee. *Econ. Geol.* **78,** 1425–1439.

ZHANG Y.-G. and FRANTZ J. D. (1987) Determination of the homogenization temperatures and densities of supercritical fluids in the system NaCl-KCl-$CaCl_2$-H_2O using synthetic fluid inclusions. *Chem. Geol.* **64,** 335–350.

ZIMMERMAN R. K. and KESLER S. E. (1981) Fluid inclusion evidence for solution mixing, Sweetwater (Mississippi Valley-type) district, Tennessee. *Econ. Geol.* **76,** 134–142.